Title: The early proximal αβ TCR signalosome distinguishes thymic selection outcome through a quantitative protein interaction network

One sentence summary: Positive and negative selection in the thymus are two dichotomous biological outcomes that are initially programmed by distinct quantitative activity through the TCR-proximal protein network.

Authors: Steven C. Neier [1,2,3]*, Alejandro Ferrer [1]*, Katelynn M. Wilton [1,2,4]*, Stephen E.P. Smith [1,5]*, April M. Huseby Kelcher [1,2,6], Kevin D. Pavelko [1], Jenna M. Canfield [7], Tessa R. Davis [1], Robert J. Stiles [1], Zhenjun Chen [8], James McCluskey [8], Scott R. Burrows [9,10], Jamie Rossjohn [11,12,13], Deanne M. Hebrink [14], Eva M. Carmona [14], Andrew H. Limper [14], Dietmar J. Kappes [15], Peter J. Wettstein [1,16], Aaron J. Johnson [1,6], Larry R. Pease [1], Mark A. Daniels [17,18], Claudia Neuhauser [19], Diana Gil [17,18,20,21], and Adam G. Schrum [17,18,20,21]

Affiliations:

[1] Department of Immunology, [2] Mayo Graduate School, Mayo Clinic College of Medicine, Rochester, MN, USA.

[3] Current address: Department of Cancer Immunology and Virology, Dana-Farber Cancer Institute, Harvard Medical School, Boston, MA, USA.

[4] Medical Scientist Training Program, Mayo Clinic College of Medicine, Rochester, MN, USA.

[5] Current address: Center for Integrative Brain Research, Seattle Children's Research Institute and Department of Pediatrics, University of Washington, Seattle, WA 98101

[6] Department of Neurology,Mayo Clinic College of Medicine, Rochester, MN, USA.

[7] Molecular Pathogenesis and Therapeutics PhD graduate program, University of Missouri, Columbia, MO, USA.

[8] Department of Microbiology and Immunology, Peter Doherty Institute for Infection and Immunity, University of Melbourne, Parkville, Victoria 3010, Australia.

[9] QIMR Berghofer Medical Research Institute, Brisbane, Australia.

[10] School of Medicine, University of Queensland, Brisbane, Australia.

[11] Infection and Immunity Program and Department of Biochemistry and Molecular Biology, Biomedicine Discovery Institute, Monash University, Clayton, Victoria 3800, Australia.

[12] ARC Centre of Excellence in Advanced Molecular Imaging, Monash University, Clayton, Victoria 3800, Australia.

[13] Institute of Infection and Immunity, Cardiff University School of Medicine, Heath Park, Cardiff CF14 4XN, UK.

[14] Thoracic Diseases Research Unit,Division of Pulmonary Critical Care and Internal Medicine, Mayo Clinic College of Medicine, Rochester, MN, USA.

[15] Blood Cell Development and Cancer Keystone, Immune Cell Development and Host Defense Program, Fox Chase Cancer Center, Philadelphia, PA 19111, USA

[16] Department of Surgery,Mayo Clinic College of Medicine, Rochester, MN, USA.

[17] Department of Molecular Microbiology & Immunology, [18] Department of Surgery, University of Missouri School of Medicine, Columbia, MO, USA.

[19] University of Minnesota Informatics Institute, Minneapolis, MN, USA.

[20] Department of Bioengineering, University of Missouri, Columbia, MO, USA.

[21] correspondence: Adam G. Schrum, email: schruma@health.missouri.edu; Diana Gil, email: gilpagesd@health.missouri.edu

* co-1st authors

Abstract

During αβ T cell development, T cell antigen receptor (TCR) engagement transduces biochemical signals through a protein-protein interaction (PPI) network that dictates dichotomous cell fate decisions. It remains unclear how signal specificity is communicated, instructing either positive selection to advance cell differentiation, or death by negative selection. Early signal discrimination might occur by PPI signatures differing *qualitatively* (customized, unique PPI combinations for each signal), *quantitatively* (graded amounts of a single PPI series), or *kinetically* (speed of PPI pathway progression). Using a novel PPI network analysis, we found that positive versus negative selection was distinguished by early TCR-proximal signals that differed *quantitatively*, but not qualitatively or kinetically. Furthermore, the signal intensity of network PPI activity was used to discover an antigen dose that caused a classic negative-selection ligand to induce positive selection of conventional αβ T cells, suggesting that the quantity of TCR triggering was sufficient to distinguish selection outcome. Since previous work had suggested that positive selection might involve a qualitatively unique signal through CD3δ, we re-examined the block in positive selection observed in CD3δ[o] mice. We found that CD3δ[o] thymocytes were inhibited but capable of signaling positive selection, generating low numbers of MHC-dependent αβ T cells that expressed diverse TCR repertoires and participated in immune responses against infection. We conclude that, rather than qualitatively enabling positive selection, CD3δ quantitatively boosts the positive selection signal for maximal generation of αβ T cells. Together, these data indicate that a quantitative network signaling mechanism through the early proximal TCR signalosome distinguishes thymic selection outcome.

Main text:

Introduction

For conventional αβ T cells, central tolerance involves positive selection of clones bearing TCRs with weak reactivity to self-peptide/MHC (pMHC), and negative selection by deletion of clones bearing TCRs with strong reactivity to self-pMHC within the thymus (*1, 2*). During selection, TCR engagement initiates biochemical signals through six associated CD3 subunits (γ, δ, 2ε, 2ζ), each containing 1-3 immunoreceptor tyrosine-based activation motifs (ITAM) and other signaling sequences (*3, 4*). CD3 activation initiates a PPI signaling cascade involving LCK, ZAP70, LAT, SLP76, and other enzymes and adaptor proteins that together form a highly interactive network, termed the proximal TCR signalosome (*5-8*). This signalosome can transmit more than one type of signal (*3, 9-13*), which may arise from the conditional interconnectivity of its multiprotein, modular network. Yet how these TCR/CD3-intrinsic and extrinsic proximal proteins form discrete network signatures that program the cellular response for positive versus negative selection is incompletely understood.

It has been proposed that signaling proteins form complexes like letters form words, with specific combinations and quantities instructing cells to perform specific functions (*14-16*). As a starting theoretical framework, basic categories of network PPI patterns that could instruct dichotomous responses in T cell selection are those in which signatures differ qualitatively, quantitatively, or kinetically (Fig. S1). In general, qualitative and kinetic signaling models are favored in the field (*2, 17-19*), whereas a former quantitative model (*20, 21*) is now thought to apply to innate-like and regulatory agonist-selected T cells more than conventional αβ T cells (*22-26*), although there is some controversy over this issue (*27-30*).

Supporting the qualitative signal model, CD3δ was shown to play a specific role in positive selection (*31, 32*). Mutation of TCR α-connecting peptide motif (αCPM) hindered association with CD3δ and blocked thymocyte development at the pre-selection CD4+ CD8+ (double-positive, DP) stage, preventing positive selection but leaving negative selection intact (*33, 34*). CD3δ° mice presented a phenotype with similarities to αCPM mutant mice, including blockade of T cell development at the pre-positive selection CD4+CD8+ DP stage (*31, 32*). All other CD3 subunits (ε, γ, ζ) are required for γδ TCR and pre-TCR signaling, making δ the only CD3 subunit that is not required until αβ TCRs are first expressed to audition for selection at the DP stage (*31*). Additionally, in FTOC experiments using wild-type OT1 thymocytes, the nominal antigenic ligand (OVA peptide in H2-Kb) was tested over ten 10-fold dilutions, in which all functional signals induced negative selection, none induced positive selection of conventional αβ T cells, and antigen dilutions that were too low for negative selection induced no selection response (*27, 35*). These and other studies showed that positive versus negative selection signals led to critical kinetic differences in Ras-Raf-ERK activation and subcellular localization downstream of the TCR signalosome (*1, 2, 32, 34-38*), supporting the proposal that TCR decides between positive and negative selection by initiating qualitatively distinct signaling pathways. Thus, the current conventional model is (I) kinetic proofreading governs TCR engagement (Ref. (*39*)), which determines (II) an as-yet-undefined quality-of-signalosome network activity that specifies positive versus negative selection, leading to (III) differential Ras-Raf-ERK activation kinetics, subcellular localization, and downstream events that program selection outcome.

The present work was dedicated to elucidating the TCR-proximal signaling step (II) above, to determine the network mechanism at play very early as protein complexes of the signalosome begin to specify selection outcome. To assess this protein network model of signal specificity in

the TCR signalosome, we employed a multiplex microsphere-based approach for analysis of 20+

cellular proteins in a 210+ matrix measuring proteins in shared complexes detected by exposed

surface epitopes (PiSCES), a system that was recently published (*40*). Based on prior knowledge

and current interactome data (*6*), we assembled a panel of immunoprecipitation (IP) antibodies

(Ab) covalently coupled to specific microsphere classes, each defined by a unique proportion of

two dyes within the polystyrene latex material base. Following various stimulatory or control

conditions, cells were lysed, multiplex IP was performed, and co-associated proteins were

probed with fluorochrome-labeled Abs and analyzed by flow cytometry (Fig. S1D; Tab. S1). In

previous studies, PiSCES analysis identified both qualitatively and quantitatively distinct

network PPI activity patterns when comparing human TCR versus CD28 signaling pathways,

and antigenic signaling in skin from autoimmune alopecia areata versus control patient T cells

(*40*). Therefore, PiSCES analysis appeared well suited to address how TCR signalosome activity

responds to different functional signals in the context of thymocyte selection.

Results

Qualitative and quantitative signaling differences in human T cell lines

To examine differences in PiSCES signatures between functionally distinct TCR signals, we

began with the LC13 system, a human TCR whose responses to agonist and antagonist pMHC

ligands are well characterized (*41-43*). Whereas LC13 TCR responds to the Epstein-Barr Virus-

derived FLRG<u>RAY</u>GL (RAY) peptide loaded in HLA-B0801 as an agonist, the single-peptide-

substituted FLRG<u>RFY</u>GL (RFY) in HLA-B0801 possesses no agonist activity, but strong

antagonist activity, despite both ligands binding LC13 TCR with similar half-lives (*41*). A

Jurkat-based cell line system was used, because (i) these cells represent transformed human

thymocytes, originating from T cell acute lymphoblastic leukemia (*44*), and (ii) in mice,

previously defined antagonist ligands were shown to induce positive selection in thymocytes,

while agonists induced negative selection (*27, 35, 45, 46*). Therefore, the LC13 TCR and human CD8 coreceptor were retrovirally expressed in JRT3 (a TCRβ-deficient derivative of Jurkat (*47*)) to create LC13ab.huCD8ab.JRT3 cells, which were stimulated with agonist peptide (RAY)-loaded C1R.B0801 antigen-presenting cells (APCs). After 5 minutes, T cells were lysed and subjected to PiSCES analysis, revealing induction of a rich network signature of multiprotein signaling complexes (Fig. 1A). To examine the extent to which two different strong agonist signals in related cell lines would produce similar PiSCES network signatures, we compared the LC13 RAY-induced PiSCES signature to our previously published dataset in which Jurkat T-cells had been stimulated for 5 minutes with Staphylococcal Enterotoxin E (SEE) superantigen (*40*). We found that many of the same protein pairs joined complexes in both sets of experiments, and we plotted the average fold-induction for protein pairs that were hits in either dataset, with SEE-Jurkat stimulation on the x-axis and agonist LC13-JRT3 stimulation on the y-axis (Fig. 1B). In a perfect correlation, all points would have fallen linearly along the 45° angle, which would have indicated that all signaling complexes were induced to the same degree in both datasets, but this was not the case. Among the differences noted, some protein pairs joined complexes that were almost exclusively induced in the SEE dataset only (Fig 1B, teal box), in a sub-network that appeared to be centered around CD28 (Fig 1C). Pursuing possible reasons for this difference, we found that unlike Jurkat, LC13ab.huCD8ab.JRT3 cells expressed low surface CD28, and thus fewer copies were available to respond to stimulation (Fig. 1D). These data provide an example where PiSCES analysis revealed qualitative and quantitative differences in cell signaling responses between two stimulatory conditions.

Human LC13 TCR signalosome activity differs quantitatively in response to agonist versus antagonist pMHC ligands

We next assessed how TCR-proximal signaling protein complexes would respond to antagonist stimulation. Initially, PiSCES network visualization of LC13 antagonist peptide (RFY) stimulation (Fig. 1E) appeared to present a lower-intensity version of the agonist (RAY)-induced signature (Fig. 1A). Comparing fold-change intensities between agonist (RAY) and antagonist (RFY) stimuli, protein complexes were induced by agonist to a quantitatively greater degree in an approximately linear fashion weighted toward agonist-stimulation, and antagonist did not appear to induce customized complexes that would indicate a qualitatively unique antagonist signature (Fig. 1F). The differences in response were sufficient to allow principal component analysis (PCA) to separate agonist (RAY)- from antagonist (RFY)-stimulated LC13 data (Fig. 1G). Thus, in contrast to that observed relative to SEE-stimulated Jurkat cells, quantitative but not qualitative differences in PiSCES signatures were evident when comparing agonist versus antagonist pMHC stimuli of LC13ab.huCD8ab.JRT3 cells.

Primary OT1 TCR signalosome activity differs quantitatively in response to stimulation by positive versus negative selection pMHC ligands

To assess PiSCES signatures of the TCR-proximal signalosome in primary pre-selection DP thymocytes, we used a mouse genotype that had previously generated data in support of the qualitative signaling model for thymic selection, and for which functionally distinct pMHC ligands have been characterized, OT1.RAG2^o.β2m^o (*27, 35*). Thymocytes were co-incubated for 1 minute with C1R.Kb APCs presenting either OVA (negative selection), Q7 (positive selection), or FARL (null, no selection) peptides, *in vitro*. After cell lysis, multiplex IP and PiSCES analysis were performed, by normalizing both OVA (Fig. 2A) and Q7 stimulation (Fig. 2B) to the null control condition, or alternatively by dividing the average MFI intensities in OVA by those of Q7 directly (Fig. 2C). With OVA stimulation, a clear network signature included shared protein complexes already being induced at 1-minute between TCR/CD3, LAT, SLP76,

GADS, PI3K, PLCγ, and others (Fig. 2A), while Q7 stimulation presented a similar network pattern but was generally weaker in both fold-change and statistical significance (Fig. 2B). Dividing average MFI intensities of hits in OVA stimulation by those of Q7 showed that fold-changes were greater in OVA-stimulation without appearance of a clear sub-network of protein complexes that might be balanced toward the Q7 positive selection stimulus (Fig. 2C). Comparing fold-change intensities between negative and positive selection stimuli, protein complexes were induced by OVA to a quantitatively greater degree in an apparent linear fashion, and Q7 did not appear to induce customized complexes that would indicate a qualitatively unique positive selection signature (Fig. 2D). These differences were sufficient for PCA to separate the response to the two stimuli (Fig. 2E). Thus, similar to the patterns observed when comparing agonist and antagonist stimulations of the human LC13 TCR, primary mouse pre-selection thymocytes responded to positive or negative selection ligands primarily via quantitatively distinct PPI activities through the proximal TCR signalosome. In contrast, if non-physiologic stimuli, pervanadate or H_2O_2, were administered to OT1.RAG2^0.β2m^0 pre-selection thymocytes, qualitatively distinct PiSCES signatures were produced (Figs. S2-S3 and Supplementary Results & Discussion), supporting the interpretation that the primarily quantitative-only network PPI differential occurred specifically in response to positive versus negative selection pMHC ligands.

We next determined the extent to which positive and negative selection pMHC stimuli induced differences in the early kinetics of PiSCES responses. For OT1.RAG2^0.β2m^0 thymocytes, PiSCES signatures began by 1 minute (Fig. 2), showing continued high activity and progression of the signature at 5 minutes (Fig. 3A-D), with waning toward early TCR-proximal signal dissolution by 15 minutes (Fig. 3E-H). At each time point, a quantitative trend was observed where the magnitude of average fold-change for induced protein pairs was greater in response to OVA than Q7 (Figs. 2D, 3D, 3H). Throughout the time course, PiSCES signatures appeared to

evolve similarly in response to OVA or Q7 stimulation. For example, for OVA stimulation, maximal TCR:LAT appearing in shared complexes occurred at 1 minute (Fig. 2A) and was reducing by 5 minutes (Fig. 3A), by which time Cbl-b was maximally induced in shared complexes with TCR, PLCγ, and Thy1, and TCR clustering began to be observed (Fig. 3A: the loop around TCR/CD3 indicates appearance of multiple copies of TCR/CD3 in shared complexes (*40*)). By comparison, in response to Q7 stimulation, the same kinetic trends were observed, but changes were of decreased relative magnitude (Figs. 2B, 3B). K-means cluster analysis of the top 15 protein pair hits revealed 3 kinetic behavior profiles in response to OVA stimulation; when applied to matching protein pairs from the Q7 stimulation condition, the same kinetic trends were preserved (Fig. 3I-J). Finally, PCA showed both types of signals expanding along an apparently common stimulation path in 3D analysis space, without obvious divergence in overall trendpath; at each kinetic time point the two stimulation conditions could be separated, with OVA response appearing somewhat farther from a zero-stimulation point (Fig. 3K). These data showed that the early kinetic PPI progression in response to a positive selection pMHC ligand was not delayed in comparison to the response to a negative selection pMHC ligand, because PiSCES signature progression evolved at a similar pace with the main difference being one of magnitude.

Because primary thymocytes responded more weakly to stimuli than did Jurkat cells, we performed the same kinetic experiments and analyses in LC13ab.huCD8ab.JRT3 cells (Figs. S4-S5), and cells transduced to express OT1 and mouse CD8 transgenes, OT1ab.muCD8ab.JRT3 cells (Figs. S6-S7). These cells were hyper-responsive when compared with primary cells, but within each cell system the same general trends were observed: quantitative differences predominated between agonist (negative selection) and antagonist (positive selection) stimuli, while substantial qualitative and early kinetic differences were not evident. Collectively, the greatest difference observed between positive and negative selection stimuli was the magnitude

of change in a common set of early TCR-proximal protein complexes (signal strength), rather than formation of unique sets of protein complexes (signal composition) or different speeds of pathway progression (signal kinetic).

PiSCES network activity predicts and confirms that early signal quantity is sufficient to distinguish thymic selection outcome

These data led to the prediction that a classic negative selection peptide should induce positive selection if the dose of its signal in responding thymocytes could be placed in the range of positive selection. To test this prediction, we used a fetal thymic organ culture (FTOC) system that had previously produced data in support of the qualitative signaling model (*27, 35*). OT1.RAG2°.β2m° fetal thymi were supplied exogenous β2m to restore MHC class I antigen presentation in conjunction with OT1-nonspecific FARL peptide for no selection (Fig. 4A), Q7 peptide for positive selection (Fig. 4B), or OVA peptide for negative selection (Fig. 4C). To directly test the quantitative hypothesis predicted by PiSCES analysis, we identified a dilute concentration of OVA (0.75 nM) that after 5 minutes of stimulation induced an approximately indistinguishable PiSCES signature from that of full-dose Q7 (10 μM). This rough equivalence was determined by dividing the response to dilute OVA by the response to full Q7 and observing that the two signals virtually canceled out (Fig. 4D), and could not be distinguished by PCA (Fig. 4E). We found that using this concentration of OVA in FTOC induced positive selection of conventional CD8αβ single-positive (SP) T cells (Fig. 4F-G). Increasing that dose by four-fold was sufficient to induce substantial generation of unconventional CD8α+ CD8β- SP T cells (Fig. 4H-I) correlating with preferential CD8αα homodimer expression (Fig. S8 and Supplementary Results and Discussion), an observation consistent with the idea that CD8αα SP T cells are generated by stronger signals than those that generate conventional CD8αβ SP T cells (*24, 25*).

In FTOCs that favored conventional positive selection, enhanced CD8αβ SP T cell viability was observed (Fig. 4J). Furthermore, when FTOC cells from positive selection conditions were subsequently stimulated with OVA-bearing APCs, T cell proliferation and development of CTL activity were observed (Fig. S9). Overall, these data support the hypothesis that quantitative network activity through the TCR signalosome provides an early instruction to specify positive- versus negative-selection in developing thymoytes.

Positive selection in CD3δ^{o} mice

Because previous work had suggested that positive selection might involve a qualitatively unique signal through CD3δ (*31-34*), we re-examined the block in positive selection observed in CD3δ^{o} mice to determine whether CD3δ's contribution might instead be quantitative, amplifying TCR/CD3 signals toward a selection threshold. As previously reported, relative to wild-type C57BL/6 (B6) mice, a severe block in positive selection and generation of CD4 or CD8 SP αβ T cells was observed upon analysis by flow cytometry of thymocytes from CD3δ^{o} mice (Fig. 5A-B). To determine if some residual positive selection was occurring in CD3δ^{o} mice, they were crossed with MHC II^{o}.β2m^{o} to generate MHC II^{o}.β2m^{o}.CD3δ^{o} mice. Although no consistent difference was observed in the percentage of CD4 or CD8 SP thymocytes between the two mutant genotypes (Fig. 5B-C, Fig. S10A-B), live cell counts showed that CD3δ^{o} mice that were MHC+ had more CD4 and CD8 SP thymocytes than MHC II^{o}.β2m^{o}.CD3δ^{o} mice (Fig. 5D-E). Consistent with the possibility that these few SP cells were being generated by positive selection, surface CD69 expression was observed on a greater percentage of thymocytes that were CD3δ^{o} than MHC II^{o}.β2m^{o}.CD3δ^{o} at stages DP (Fig. 5F-I) and CD4 or CD8 SP (Fig. S10C-J). To isolate the ability of the thymus to generate SP cells, FTOC was performed, where a greater percentage of CD4 SP cells was generated in CD3δ^{o} than MHC II^{o}.β2m^{o}.CD3δ^{o} thymi (Fig. S10K-O). Analysis of CD4 and CD8 splenic T cells confirmed that CD3δ^{o} mice had low cell numbers

relative to B6, but such cells were absent in MHC II°.β2m°.CD3δ° mice (Fig. 5J-N). Compared with B6, CD3δ° splenic T cells expressed less CD5, indicative of having undergone weaker selection signals (48), and most CD3δ° T cells were CD24-low and PNA-low staining, consistent with the progressive differentiation expected to occur post-selection (Fig. S11). Because in CD3δ° thymocytes, signaling occurred (resulting in CD69 induction) in an MHC-dependent manner to generate low-count SP cells in the thymus and periphery, we conclude that a low level of positive selection still occurred in these mice.

To test the hypothesis that a specific TCR lacking CD3δ° could mediate some amount of positive selection *in vivo*, we generated OT1.RAG2°.CD3δ° and OT1.RAG2°.β2m°.CD3δ° mice. Compared with OT1.RAG2° mice, OT1.RAG2°.CD3δ° mice showed a reduction in peripheral blood T cells; however, their low T cell number was dependent on MHC class I-mediated survival, because peripheral blood T cells were absent in OT1.β2m°.RAG2°.CD3δ° mice (Fig. S12). We conclude that a low amount of positive selection still appeared to be active when single-TCR-expressing cells lacked CD3δ.

To directly test the hypothesis that a specific TCR lacking CD3δ° could transduce a positive selection signal, we compared OT1.RAG2°.β2m° and OT1.RAG2°.β2m°.CD3δ mice in FTOC. As expected for OT1.RAG2°.β2m° thymocytes, FARL peptide induced no selection (Fig. 6A), Q7 peptide induced positive selection (Fig. 6B), and OVA peptide induced negative selection of (Fig. 6C). In contrast, OT1.RAG2°.β2m°.CD3δ° thymocytes failed selection with Q7 peptide (Fig. 6D-E), but underwent positive selection in response to OVA peptide (Fig. 6F), producing conventional CD8αβ SP T cells (Fig. 6G-H). Having observed these selection outcomes, we

examined the ability of pre-selection OT1 thymocytes to induce TCR signal transduction +/-

CD3δ in response to positive selection pMHC ligands. To maximize sensitivity to small

signaling changes (by minimizing multiple-hypothesis statistical correction) in the severely low-

TCR expressing OT1.RAG2^0.β2m^0.CD3δ^0 thymocytes, these PiSCES experiments were limited to

a small collection of strongly inducible protein pairs. We found that 5-minute stimulation of pre-

selection OT1.RAG2^0.β2m^0 thymocytes with Q7 peptide presented by C1R.Kb APCs induced

multiple copies of TCR/CD3 to join shared complexes, an expected consequence of receptor

crosslinking (visualized as a loop around TCR/CD3, Fig. 6I). TCR also appeared in shared

complexes with LAT, GADS, PI3K, Cbl-b, and others. By comparison, stimulation of pre-

selection OT1.RAG2^0.β2m^0.CD3δ^0 thymocytes with OVA peptide also induced those protein

complexes (Fig. 6J); however, the network signature of CD3δ^0 cells responding to OVA was

mostly weaker, with fewer statistically significant hits (statistically non-significant comparator

trends shown with dashed lines, Fig. 6J), with most heteroprotein associations being of weaker

intensity than those seen for OT1.RAG2^0.β2m^0 thymocytes responding to Q7 peptide. We

conclude that the OT1 TCR was capable of transducing a positive selection signal +/- CD3δ,

although when expression of both TCR (CD3δ^0) and MHC (β2m^0) were severely low in FTOC,

positive selection required a strong pMHC ligand.

Diverse αβ TCR repertoire in peripheral CD3δ^0 T cells

Perhaps CD3δ supplied a qualitative positive selection-specific signal that, as a general rule, was

required by the vast majority of T cell clones; in that case, in the absence of CD3δ, residual

positive selection could be explained if it were due to a few clones with rare, unusual CD3δ-

independent TCRs. If correct, then peripheral, polyclonal CD3δ^0 T cells should display a

relatively limited TCR repertoire. Alternatively, if the main role of CD3δ was to quantitatively

enhance positive selection signals, then peripheral CD3δ T cells might display a diverse TCR repertoire even though there were few T cells, because selection signals from all clones would be inhibited equally. To distinguish between these two disparate predictions, we utilized a mouse TCRβ repertoire diversity matrix system in which real-time PCRs were performed for 252 fully nested BV-BJ combinations of 21 BV primers and 12 BJ primers (*49*). This system allowed repertoire diversity of T cell populations to be assessed at a substantially deeper level than standard V-gene spectratyping, by comprehensively assessing all possible V-J combinations. We found that specific TCRβ transcripts tended to be decreased in quantity from CD3δ° relative to B6, as expected due to their decreased peripheral T cell number in the mutant, but strikingly, both CD3δ° and B6 were capable of expressing highly diverse repertoires (Fig. 7A-B; Fig. 13). Importantly, there was no evidence of a limited number of BV-BJ combinations in CD3δ°. The diversities of the 252 BV:BJ combinations were estimated by scaled Shannon entropy under conditions where B6 input RNA was decreased relative to CD3δ° RNA so that samples would provide comparable T cell representation despite the lower T cell number in mutant spleens. Scaled Shannon entropy is a value whose range is 0-1, where 0 represents minimum diversity exhibited by a monoclonal T cell population, and 1 represents maximal repertoire diversity when all BV:BJ combinations are expressed equally (*49*). Entropy values for two B6 mice were 0.74 and 0.64, while those of two CD3δ° mice were in a similar range, 0.67 and 0.68, indicating that the two genotypes were both capable of generating a diverse TCRβ repertoire in the periphery.

Because it is the TCRα subunit that shares a positive selection signaling axis with CD3δ (*33, 34*), we also assessed peripheral TCRα diversity with a spectratype survey of 16 Vα genes using previously published primers and methods (*50, 51*), and observed similar expression patterns between CD3δ° and B6 genotypes (Fig. 7C). We conclude that positive selection in the absence of CD3δ occurs for a population of T cells expressing substantial repertoire diversity with usage

of numerous TCRα and TCRβ genes. These data do not provide evidence that CD3δ supplies a qualitatively distinctive signal that would be required as a general rule for positive selection. Instead, it appears that diverse TCRs can signal positive selection without CD3δ, but clones expressing these TCRs have a poor success rate, implying that the role of CD3δ is to quantitatively enhance positive selection to maximize the generation of peripheral T cells.

Immune function of αβ CD3δ T cells

To test the function of the diverse MHC-dependent αβ T cell pool that was positively selected in CD3δ mice, they were challenged with two infections known to require αβ T cells for survival. These were (i) *Pneumocystis* fungal pulmonary infection causing pneumonia (PCP), an infection that is fatal in CD4-depleted hosts such as AIDS patients (*52*), and (ii) Theiler's Murine Encephalomyelitis Virus (TMEV), an infection whose clearance in mice normally requires CD4 and CD8 T cells to prevent acute encephalitis and paralysis (*53*).

Mice from the following genotypes were infected with PCP: B6, MHC II.β2m (MHC-deficient), CD3εζ (T cell and TCR/CD3-deficient, lacking expression of all four CD3 genes (*54*)), and CD3δ. Both B6 and CD3δ genotypes were resistant to PCP with 100% survival, whereas MHC-deficient and other T cell-deficient mice were susceptible and succumbed (Fig. 8A), with accompanying symptoms of pneumonia including weight loss (Fig. 8B), increased lung weight, indicative of fluid accumulation (Fig. 8C), and decreased blood oxygen saturation, indicating loss of respiratory function (Figure 8D). To test the hypothesis that CD4 T cells were required for PCP resistance in CD3δ mice, we compared PCP infection of CD3δ mice that were depleted of CD4 T cells through weekly injections of mAb GK1.5 anti-CD4, with CD3δ mice that had received control PBS injections. We found that CD4-depleted CD3δ mice were

susceptible and succumbed to PCP infection, similar to other susceptible genotypes, including T cell-deficient $CD3\epsilon^o\zeta^o$ mice, and $OT1.RAG2^o$ mice expressing a single PCP-irrelevant transgenic TCR, while PBS-injected $CD3\delta^o$ mice and B6 mice were resistant with 100% survival (Fig. S14). Antigen presentation was required for PCP resistance, because $MHC\ II^o.\beta2m^o$ and $MHC\ II^o.\beta2m^o.CD3\delta^o$ mice were susceptible and succumbed with symptoms of pneumonia (Fig. 8E-H). We conclude that the low numbers of positively selected CD4 T cells in $CD3\delta^o$ mice were able to express MHC-dependent immune activity.

To assess CD8 T cell function, mice from the following genotypes were infected with TMEV: B6, $CD3\delta^o$, $CD3\epsilon^o\zeta^o$ (T cell-deficient), and $OT1.RAG2^o$ (containing a single TMEV-irrelevant TCR transgenic CD8 T cell population). Both B6 and $CD3\delta^o$ genotypes were resistant to TMEV infection with 100% survival, whereas T cell-deficient and $OT1.RAG2^o$ mice were susceptible, suffering functional deficit that was measured by loss of RotaRod performance (Fig. 9A-B). To determine which T cell subsets contributed to protection from TMEV of B6 and $CD3\delta^o$ mice, we compared infection of mice that were either (i) depleted of CD4 T cells through weekly injections of mAb GK1.5 anti-CD4, (ii) depleted of CD8 T cells through weekly injections of mAb 2.43 anti-CD8, (iii) both CD4 and CD8 T cell-depleted, or (iv) non-depleted, control PBS-injected. Whereas B6 mice only succumbed upon depletion of both CD4 and CD8 T cells, as expected (*53*), $CD3\delta^o$ mice succumbed upon depletion of either subset (Fig. 9C-H). These data suggest that $CD3\delta^o$ mice are immune compromised relative to wild-type B6 mice, as expected, but the low-count peripheral $CD3\delta^o$ CD4 and CD8 T cells participate in protective immune activity against infection.

Discussion

Life versus death represents a qualitative difference, which creates the expectation that a qualitative difference in signal transduction must specify these outcomes when they are programmed cellular responses. We have presented the possibility of qualitative, quantitative, or kinetic differences in early TCR-proximal network PPI signaling activity in a framework that considers them to be opposing models to be distinguished from each other. Historically, that original framework was useful and warranted, since the signals that decide thymic selection have been proposed to originate from TCR-proximal signaling elements with qualitative properties, including special subunits such as CD3δ (*31, 32*), motifs such as TCR αCPM (*33, 34*), patterns of immunoreceptor tyrosine-based activation motif (ITAM) phosphorylation (*10, 55-58*), and other possible candidates that might specify selection outcome (*59, 60*). The present data suggest that a major role in selection for players such as these may be to affect the initial quantity of signal transmitted through the proximal TCR signalosome, rather than to create unique combinations of TCR-proximal protein complex intermediates during the earliest selection signals. The data are compatible with a quantitative signaling model that has been proposed (*61, 62*), where a single TCR signaling signature may be active at sub-threshold level in the basal state, and different signals are transduced as (i) CD3 subunit multiplicity and activity mostly provide quantitative information of ligand binding strength, (ii) the balance of signaling activity is perturbed away from the basal state, and (iii) a series of quantitative thresholds demarcates separate functional instructions.

Interestingly, the present data imply that early signal translation between two kinetic parameters (initially TCR engagement, later Ras-Raf-ERK activity) is mediated by this quantitative network parameter that specifies positive versus negative selection based on the accumulation or frequency of a single-series (and single-kinetic) network PPI signature that propagates through the early proximal TCR signalosome upon productive engagement by a pMHC ligand. This hypothesis was generated by PiSCES analysis, which identifies signatures of targeted sub-

networks, but does not comprehensively assess all proteins, lipids, and other molecules that contribute to the signal (63). Therefore, it was formally possible that key qualitatively distinct molecular species that instruct selection early were being missed, if such key species did not affect the sub-network being measured. We reasoned that the only way to determine whether the entire signaling network responded according to the quantitative principle predicted by PiSCES was to test that principle functionally. Upon doing so, we identified a specific, low concentration of OVA, a classic negative-selection peptide in the OT1 system, which induced positive selection of conventional T cells. This principle was corroborated a second way, when reducing TCR signaling strength in the context of CD3δ^o and $\beta2m^o$ allowed high-dose OVA to induce positive selection of conventional OT1 T cells. These data support the conclusion that a predominantly quantitative network signaling mechanism is sufficient to provide an early instruction that culminates in determination of thymic selection outcome.

Previously, there was already definitive data showing that dilution of OVA peptide did not induce positive selection of conventional OT1 T cells across 10-fold dilutions in FTOC (27, 35), and this supported the idea that signaling quantity was insufficient to explain the difference between positive and negative selection. In the present work, the specific dilution of OVA peptide that induced positive selection of conventional $\alpha\beta$ T cells in FTOC falls almost midway between the two closest log-dilutions that were previously published. Thus, the present data are compatible with the previous conclusion that peptide affinity is the master driver of selection outcome across a wide range of concentrations. But the new lesson learned is that a key early proximal network PPI signaling parameter that is controlled by peptide affinity is quantitative in nature.

CD3δ plays a critical role in positive selection, and in absence of this subunit a poorly populated peripheral αβ T cell pool is generated that results in immune compromise in mice. That CD3δ might provide a qualitative subunit-specific distinctive signal required for positive selection was an attractive possibility for many reasons, including the fact that if one wished to control positive selection and central tolerance pharmacologically, pathways could be more easily targeted with specificity if qualitatively distinctive intermediates were involved. Our data began to diverge from this possibility when it was found that the few αβ T cells known to be present in CD3δ⁰ mice (*31*) did not represent a secondary "leakiness" effect in the face of a strong developmental block, but rather these cells were products of residual signaling- and MHC-dependent positive selection (Figs. 5-6). Strikingly, CD3δ⁰ and wild-type B6 mice both exhibited high diversity in rearranged TCRβ and TCRα genes in the peripheral T cell pool (Fig. 7), and those T cells participated actively in CD4-dependent and CD8-dependent T cell responses to infection (Figs. 8-9). These data are most easily explained if, as a general rule, CD3δ does not provide a subunit-specific qualitatively distinctive signal required for positive selection.

The model most consistent with the data is that CD3δ quantitatively boosts the positive selection signal to increase the number of T cells generated from a diverse repertoire of candidate αβ TCR-bearing clones (*64*). This function could be partially due to the fact that the presence of CD3δ improves TCR/CD3 folding and increases surface expression, which may contribute to quantitatively increasing signals. This possibility is consistent with the previously reported observation that positive selection was rescued in CD3δ⁰ mice by a CD3δ-mutant transgene that restored surface TCR/CD3 expression levels but carried a non-functional ITAM (*32*). Under a qualitative signaling model, the non-ITAM CD3δ motif that might provide the specificity for positive selection remained mysterious, but in a quantitative model, provision by CD3δ of

optimal native TCR/CD3 assembly and expression could play a major role. Furthermore, models in which CD3δ acts in concert with αCPM and CD4 or CD8 coreceptors to mediate positive selection (*65*) are compatible with the present proposal that a main outcome of these interactions is to boost signal intensity. We conclude that the main functional signal for positive selection contributed by CD3δ is not qualitatively distinctive, but rather involves quantitative amplification to maximize the number of αβ T cells that populate the peripheral immune system.

In light of the present data, we propose that the framework of the original question should be restructured. Quantitative and kinetic differences in PPI signaling networks are not mutually exclusive of, nor incompatible with, a qualitative signaling model, if we allow a broader definition. To express unique combinatorial patterns of protein associations is only one way to transmit a qualitatively distinctive signal, and the present study did not find evidence for this in the early proximal TCR signalosome in the context of selection. Instead, this work emphasizes that quantitative and kinetic differences are both subtypes of qualitative differences, which can contribute to molecular logic circuits that specify instructive signals (*66*). Positive versus negative selection appears to represent an example of this network principle, which programs a dichotomous cell-fate decision that is fundamental to generating a centrally tolerant adaptive T lymphocyte population.

Materials & Methods

Experimental design

Sample size was determined by precedent observations and sample availability. All cellular flow cytometry was performed at least in duplicate in each experiment, which allowed for calculation of central values, proportions, SD, and SEM. For *in vitro* signaling experiments,

inter-experimental n was decided to be at least 3 *a priori,* which was previously determined to be optimal for multiplex PiSCES experiments (*40*). For FTOC experiments, because the number of pregnancies and fetuses could not be perfectly controlled, the final decision on the number of cultures dedicated to any one condition occurred on the day of fetal harvest, at which time all fetuses judged to be macroscopically healthy were used in experiments. For experiments that assessed survival of infection, the minimum was three mice per experimental group, a decision that was based on our own unpublished data, as follows. Previous to performing the controlled infection experiments reported here, we observed that when natural, uncontrolled PCP infection killed many immune compromised mice in our colonies in our animal facility, CD3δ^0 mice were spared. We co-housed CD3δ^0 mice that had survived natural infection with new mice from susceptible strains such as CD3$\epsilon^0\zeta^0$, and found that susceptible-genotype cage mates died of PCP.

These preliminary experiments caused us to hypothesize that 100% of CD3δ^0 mice would survive controlled PCP infection, such that setting experiment longitude to at least 150 days (for PCP infection) would allow statistical significance to be achieved with at least 3 mice per genotype. We carried that choice of minimum mouse n per experiment to TMEV infection, where 100% survival of CD3δ^0 mice would be statistically significant if experiments lasted at least 30 days. We routinely prepared more mice per experimental group when age/sex matching and cost permitted.

Rules for stopping data collection. All assay endpoints were decided in advance, except in the case of infection experiments. When CD3δ^0 mice survived infections, we allowed experiments to continue longer than is common practice for controlled PCP and TMEV acute infections, in case the CD3δ^0 mice might succumb if given more time, although this outcome was not observed.

Inclusion and exclusion criteria. All criteria were established prospectively. All data were included in the analyses, with one exception in *in vivo* infection experiments. If an immune

compromised mouse died but cause of death was not experimental infection, that mouse was excluded from analysis. Examples of excluded mice include any that died within 3 hours of TMEV injection, or for PCP infection, mice that died outside the infection time course indicated by the controls and without symptoms of pneumonia. There was no identification or exclusion of outliers from any data set.

Research objectives. Hypotheses as stated in the text were pre-specified before performing all experiments, with one exception. For TCR repertoire analysis, although the overall hypothesis was pre-specified, we did not decide how to present the analysis of the hypothesis until after data was acquired and underwent initial analysis. This is because we realized that we preferred not to analyze averages from the data of all mice tested (which would inflate Shannon entropy, and would appear to support our final interpretation, a point that is discussed in Supplementary Materials & Methods).

Research subjects. Mice of B6 background were used in experiments. Transgenic and knockout mice are specified in the corresponding experiments and in the subsection "Mice" below. This study used controlled laboratory experiments, with specific details outlined in the corresponding sections of the text, in bibliographic references, and in the following sections. Individual mice were chosen without subjective or objective pre-characterization. There was no blinding step during any experiments.

Cell lines

JRT3-T3.5 (ATCC TIB-153) cells were purchased from ATCC. The LC13 system, including LC13ab.huCD8ab.JRT3 cells and C1R.HLA-B0801 (C1R.B08) antigen presenting cells (APC) were described previously (*41-43, 67, 68*). We generated OT1ab.muCD8ab.JRT3 cells using retroviral transduction of previously published OT1 sequences (*69*) that were provided by Dario Vignali (then at St. Jude Children's Research Hospital, Memphis, TN), and mouse CD8 genes

isolated from cDNA. All cells were grown in RPMI media (Life Technologies) with 10% Cosmic Calf serum (Hyclone), 2 mM L-glutamine (Life Technologies), and 100 U/mL Penicillin/100 μg/mL Streptomycin (Life Technologies), and maintained in a 37ºC incubator with 5% CO_2.

Mice

All mice were B6 background. CD3δ° mice originated from Fox Chase Cancer Center. CD3εζ° mice, which lack expression of all four CD3 genes (*54*), were originally provided by Dario and Kate Vignali (then at St. Jude Children's Research Hospital, Memphis, TN) with permission from Cox Terhorst (Beth Israel Deaconess Medical Center, Harvard Medical School, Boston, MA). β2m° mice were obtained from The Jackson Laboratory, as were MHC II° in which all conventional MHC class II genes are deleted (*70*). All genetically engineered mouse strains were bred and maintained at Mayo Clinic and University of Missouri-Columbia, and all animals were housed in specific pathogen-free facilities. In general, mice were used at 6-12 weeks of age, and within experiments were age and sex matched between experimental groups. Individual mice within 15 days of age were accepted as age-matched. Mice used in infection experiments were age- and sex-matched between experimental groups, and began experiments at 8-16 weeks of age, except for OT1.RAG2° mice, which served as infection-susceptible controls without age- and sex-matching. All mouse care and experimentation adhered to institutional guidelines and the NIH Guide for the Care and Use of Laboratory Animals.

Antibodies and staining reagents

For cellular flow cytometry, mAbs included: Thy1.2/CD90 (30-H12, Biolegend), TCRβ (H57, eBioscience), Vα2 (B20.1, BD), CD3ε (145-2C11, Biolegend), CD8α (53.6.7, Biolegend),

CD8β (53-5.8, Biolegend), CD4 (GK1.5, BD Biosciences), CD69 (H1.2F3, Biolegend), CD24 (M1/69, Biolegend), CD5 (53-7.3, Biolegend). Other binding reagents included: Peanut Agglutinin (PNA)-FITC (Sigma-Aldrich), Streptavidin-PE and -APC-Cy7 (Biolegend), H-2Kb-SIINFEKL (OVA) tetramer, and Thymic Leukemia Antigen (TLA) tetramers (NIH tetramer core facility). For multiplex IP and PiSCES analysis, anti-mouse Abs are listed in Table S1, while a similar table for anti-human Abs used in conjunction with Jurkat and JRT3 cell lines was previously published (40).

Organ processing and flow cytometry

Whole thymocyte or splenocyte single-cell suspensions were prepared for analysis as previously described (71). Cells were analyzed by flow cytometry using either BD Biosciences LSR II or Accuri C6 instruments.

Cell stimulation and lysis

To prepare APCs for T cell stimulation, C1R cells were incubated with specific peptides for 2 hours in serum-free RPMI at 37ºC. For the LC13 system, C1R.B08 cells were used as APCs, with agonist peptide (FLRGRAYGL), antagonist peptide (FLRGRFYGL), or no peptide. For OT1 systems, C1R.Kb cells were used as APCs, with peptides FARL (SSIEFARL), Q7 (SIINFEQL), or OVA (SIINFEKL). Peptide-loaded APCs were washed once in PBS, then fixed by re-suspension in 0.05% gluteraldehyde in PBS, as previously described (34). After 30 seconds, fixation was halted by the addition of 200 mM glycine/PBS, and fixed cells were washed three times in PBS. Responding T cells included LC13ab.huCD8ab.JRT3, OT1ab.muCD8ab.JRT3, or primary pre-selection DP thymocytes of OT1.β2m$^{\circ}$.RAG2° or OT1.β2m$^{\circ}$.RAG2°.CD3δ° genotypes. JRT3-based cell lines were used after having been placed in

fresh media at 0.35 x 10^6 per mL in tissue culture the previous evening. The day of stimulation,

15 x 10^6 T cells were resuspended in 200 μL ice-cold PBS, mixed with 20 x 10^6 APCs in an equal

volume of ice-cold PBS, and centrifuged for 5 minutes at 300g at 4ºC to facilitate cell

conjugation. Supernatant was discarded, and stimulation commenced as the T cell/APC pellet

was placed in a 37ºC water bath for the indicated amount of time before being flash-frozen in

liquid nitrogen. Control unstimulated T cells were mixed with non-loaded (LC13 system), or

null-peptide-loaded (OT1 system) fixed APCs in parallel. Frozen cell pellets were either lysed

immediately or stored briefly at -80ºC before being lysed in lysis buffer (150 mM NaCl, 50 mM

Tris pH 7.4, 1% Digitonin (High Purity, Millipore), 1X Halt protease/phosphatase inhibitors

(Pierce), 10 mM NaF, 2 mM Sodium Orthovanadate, 10 mM Iodoacetamide).

Multiplex capture and probe of protein complexes

In the TCR signalosome, complete analysis involved 20 signaling proteins that were targeted in a

minimum 20 x 20 matrix of capture/probe antibodies (Tab. S1). This generated a minimum of

400 protein co-association measurements, including 210 total unique protein co-associations:

[((20 capture X 20 probe) – 20 homotypic combinations) / 2] + 20 homotypic combinations =

210. In some experiments where noted, only 8 proteins were targeted, with commensurate

reduction in the matrix. Some experiments included capture/probe combinations targeting

additional proteins beyond the 20 described in Tab. S1, but their data are not visualized because

they were not assessed in all experiments. Procedures followed published protocols (40). Briefly,

a master mix containing equal numbers of each antibody-coupled Luminex bead class was

prepared and distributed into post-nuclear lysate samples in duplicate. Protein complexes were

immunoprecipitated from samples overnight, washed twice, and distributed into as many wells of

a 96-well plate as there were probes. Probe antibodies were added and incubated for 1 hour, with

gentle agitation at 500 RPM in a cold room, followed by three more washes. Biotinylated probe

antibody wells were then incubated 30 minutes with streptavidin-PE. After three final washes,

microbeads were resuspended in 125 μL and fluorescence data were acquired on a Bioplex-200 instrument that was calibrated according to manufacturer recommendations, and run on the "high RP target" setting. Data files were exported in both Microsoft Excel and XML formats for further processing.

Fetal Thymic Organ Culture (FTOC)

Timed matings were performed as previously described (*72*). Briefly, mouse cages were divided in half using an acrylic divider, with adequate food and water available on each side. One male and one female resided on each side of a divided cage for ~72 hours, after which the divider was removed in late afternoon to make mating possible overnight. Fetal thymic organ culture was performed as previously described (*35*). On embryonic day (e)15, carbon dioxide was used to euthanize mothers and fetal thymi were harvested. Each fetal thymic lobe was placed on sterile mixed cellulose ester gridded filter paper (Millipore) on top of a Gelfoam sterile sponge (Pfizer), in Hyclone CCM1 Serum Free media (GE Life Sciences) in one well of a 48- or 96-well plate. Some cultures were supplemented with exogenous human β2m (5 μg/mL, Sigma) and peptides FARL, Q7, or OVA at the indicated concentrations. Tissue culture occurred at 37ºC for seven days prior to harvest and assessment of thymic selection by flow cytometry.

TCR Repertoire Analysis

TCRα spectratype analysis was performed with primer sequences and protocols as previously described in detail (*50, 51*). The diversity of TCRβ repertoires was evaluated by a previously described matrix that assesses all possible BV-BJ combinations (*49*). Briefly, TCRβ transcripts were reverse-transcribed from total RNA with a biotinylated BC region reverse primer and

amplified with pools of BV-specific forward primers. The resulting amplicons were mixed with streptavidin-coated magnetic beads to enrich products that included the biotinylated BC region primer. The bead-enriched products were delivered to microtiter wells for amplification in real-time PCRs using 252 fully nested BV-BJ combinations of 21 BV primers and 12 BJ primers (see Supplementary Materials & Methods).

Pneumocystis murina infection causing pneumonia (PCP)

Mice were fed mouse chow containing Trimethoprim Sulfamethoxazone for 3 weeks to clear possible previous infections (*73*), then allowed two weeks to clear the medication (*74*). Throughout experimentation, mice were maintained on 500 mg/L antibiotic regimen in drinking water, alternating monthly between cephalexin and amoxicillin. Mice were intranasally infected with 0.5 x 10^6 *Pneumocystis murina* cysts (ATCC) intranasally on day 0 and day 7 and monitored for 20% weight loss and subjective moribund characteristics resulting from *Pneumocystis* pneumonia. Prior to sacrifice, blood oxygen saturation was measured to indicate compromise of pulmonary function and active pneumonia via the MouseOx System (Starr Life Sciences, Oakmont, PA). Upon sacrifice via carbon dioxide asphyxiation, lungs were weighed to assess general fluid influx into lung parenchyma. Mice that did not reach a terminal endpoint were allowed to live a minimum of 150 days. Depletion of CD4 T cells was accomplished by i.p. injection of 0.3 mg GK1.5 mAb (BioXcell, New Lebanon, NH; or PBS control) on days -4 and -1 prior to infection, and weekly thereafter. Depletion status was monitored by flow cytometric analysis of blood periodically throughout the experiment.

Theiler's Murine Encephalomyelitis Virus (TMEV) infection

Age- and sex-matched mice were weighed and trained on a RotaRod apparatus daily for 3 days before intracranial infection with two million plaque forming units of TMEV (Daniel's strain), as

previously described (*75*). Mice were regularly monitored for 20% weight loss, moribund characteristics, and declining neurological function via decreased RotaRod performance. Depletion of CD4 and/or CD8 T cells was accomplished by i.p. injection of 0.3 mg of each mAb (GK1.5 anti-CD4, 2.43 anti-CD8, BioXcell, New Lebanon, NH; or PBS control) on days -3 and -1 prior to infection, and weekly thereafter. Depletion status was monitored by flow cytometry analysis of blood periodically throughout the experiment.

PiSCES analysis

PiSCES analysis was previously described in detail (*40*). XML output files were parsed to acquire the raw data for use in MATLAB, R statistical package, Cytoscape, and other analysis/visualization platforms. For each well from an experiment's data acquisition plate, data were processed in order to (i) eliminate doublets based on the doublet discriminator intensity (>5,000 & <25,000 arbitrary units, Bioplex-200), (ii) identify specific bead classes within the bead regions used, and (iii) pair individual bead PE fluorescence measurements with their corresponding bead region. This processing generated a distribution of PE intensity values for each pairwise protein PiSCES measurement. Adaptive non-parametric with empirical cutoff (ANC) analysis was used as the primary method to determine statistical significance of PiSCES data, as previously described (*40*). Briefly, differences in specific protein-pair PiSCES measurements were considered hits if they were consistently identified as significant in 100% of experiments, with the minimum number of experiments per experimental condition set as three. An overall type I error of 0.05 was set as the cutoff for statistical significance, which incorporated a Bonferroni adjustment for multiple hypotheses. Principal component analysis (PCA) was performed using the built-in function in MATLAB, using as input variables the log2 median fluorescence intensity (MFI) of each PiSCES measurements performed, where each stimulation condition in one experiment constituted an observation. PiSCES analysis by PCA used complete datasets from all experiments. In contrast, node-edge diagrams only visualized

subsets of data, and were generated using the publicly free open network resource, Cytoscape. For protein pairs that had multiple measurements targeting different epitope combinations, the measurement with the greatest mean-log2 fold-change was selected for node-edge diagram visualizations.

Other statistical analyses

For kinetic analysis, the mean absolute value log2 fold change across each time point measured and across both stimulation conditions (OVA/FARL and Q7/FARL, or RAY/Null and RFY/Null) were used to select the top 15-20 protein pair hits. K-means clustering was performed in MATLAB using Squared Euclidean as the distance measurement on log2 fold changes expressed as % max change across the kinetic. The cluster number was selected to maximize the number of distinct kinetic patterns for a given experimental system. Clustering was performed on the negative selection ligand or agonist stimulation and then data from the positive selection ligand or antagonist stimulation were mapped onto these clusters to compare the overall signaling kinetics. Statistical analysis of FTOC data was performed using two-tailed Student's t-tests with GraphPad Prism software. Paired data originated from single fetal thymi whose two lobes were separated for culture in OVA peptide or matched-dose FARL peptide. Other statistical analyses between groups were completed using unpaired, one- or two-tailed Student's t-tests. Survival analysis was completed using the Log-Rank (Mantel-Cox) statistical test. Statistical significance was defined as P-value < 0.05 α-cutoff.

References & Notes

1. K. A. Hogquist, T. A. Baldwin, S. C. Jameson, Central tolerance: learning self-control in the thymus. *Nat Rev Immunol* **5**, 772-782 (2005).
2. G. Werlen, B. Hausmann, D. Naeher, E. Palmer, Signaling life and death in the thymus: timing is everything. *Science* **299**, 1859-1863 (2003).
3. C. S. Guy, D. A. Vignali, Organization of proximal signal initiation at the TCR:CD3 complex. *Immunol Rev* **232**, 7-21 (2009).

4.   A. Borroto, D. Abia, B. Alarcon, Crammed signaling motifs in the T-cell receptor. *Immunol Lett* **161**, 113-117 (2014).

5.   G. Werlen, E. Palmer, The T-cell receptor signalosome: a dynamic structure with expanding complexity. *Curr Opin Immunol* **14**, 299-305 (2002).

6.   R. Roncagalli, S. Hauri, F. Fiore, Y. Liang, Z. Chen, A. Sansoni, K. Kanduri, R. Joly, A. Malzac, H. Lahdesmaki, R. Lahesmaa, S. Yamasaki, T. Saito, M. Malissen, R. Aebersold, M. Gstaiger, B. Malissen, Quantitative proteomics analysis of signalosome dynamics in primary T cells identifies the surface receptor CD6 as a Lat adaptor-independent TCR signaling hub. *Nat Immunol* **15**, 384-392 (2014).

7.   L. Balagopalan, R. L. Kortum, N. P. Coussens, V. A. Barr, L. E. Samelson, The Linker for Activation of T Cells (LAT) Signaling Hub: From Signaling Complexes to Microclusters. *J Biol Chem* **290**, 26422-26429 (2015).

8.   S. V. Pageon, T. Tabarin, Y. Yamamoto, Y. Ma, J. S. Bridgeman, A. Cohnen, C. Benzing, Y. Gao, M. D. Crowther, K. Tungatt, G. Dolton, A. K. Sewell, D. A. Price, O. Acuto, R. G. Parton, J. J. Gooding, J. Rossy, J. Rossjohn, K. Gaus, Functional role of T-cell receptor nanoclusters in signal initiation and antigen discrimination. *Proc Natl Acad Sci U S A* **113**, E5454-5463 (2016).

9.   J. Sloan-Lancaster, B. D. Evavold, P. M. Allen, Induction of T-cell anergy by altered T-cell-receptor ligand on live antigen-presenting cells. *Nature* **363**, 156-159 (1993).

10.   J. Madrenas, R. L. Wange, J. L. Wang, N. Isakov, L. E. Samelson, R. N. Germain, Zeta phosphorylation without ZAP-70 activation induced by TCR antagonists or partial agonists. *Science* **267**, 515-518 (1995).

11.   E. Teixeiro, M. A. Daniels, B. Hausmann, A. G. Schrum, D. Naeher, I. Luescher, M. Thome, R. Bragado, E. Palmer, T cell division and death are segregated by mutation of TCRbeta chain constant domains. *Immunity* **21**, 515-526 (2004).

12.   G. Altan-Bonnet, R. N. Germain, Modeling T cell antigen discrimination based on feedback control of digital ERK responses. *PLoS Biol* **3**, e356 (2005).

13.   E. Teixeiro, M. A. Daniels, S. E. Hamilton, A. G. Schrum, R. Bragado, S. C. Jameson, E. Palmer, Different T Cell Receptor Signals Determine CD8+ Memory Versus Effector Development. *Science* **323**, 502-505 (2009).

14.   N. L. Komarova, X. Zou, Q. Nie, L. Bardwell, A theoretical framework for specificity in cell signaling. *Mol Syst Biol* **1**, 2005 0023 (2005).

15.   J. Jin, T. Pawson, Modular evolution of phosphorylation-based signalling systems. *Philos Trans R Soc Lond B Biol Sci* **367**, 2540-2555 (2012).

16.   A. G. Schrum, D. Gil, Robustness and Specificity in Signal Transduction via Physiologic Protein Interaction Networks. *Clinical & experimental pharmacology* **2**, S3 001 (2012).

17.   J. I. Elliott, T cell repertoire formation displays characteristics of qualitative models of thymic selection. *Eur J Immunol* **27**, 1831-1837 (1997).

18.   T. K. Starr, S. C. Jameson, K. A. Hogquist, Positive and negative selection of T cells. *Annu Rev Immunol* **21**, 139-176 (2003).

19.   H. J. Melichar, J. O. Ross, P. Herzmark, K. A. Hogquist, E. A. Robey, Distinct temporal patterns of T cell receptor signaling during positive versus negative selection in situ. *Science signaling* **6**, ra92 (2013).

20.   P. G. Ashton-Rickardt, S. Tonegawa, A differential-avidity model for T-cell selection. *Immunol Today* **15**, 362-366 (1994).

21.   E. Sebzda, V. A. Wallace, J. Mayer, R. S. Yeung, T. W. Mak, P. S. Ohashi, Positive and negative thymocyte selection induced by different concentrations of a single peptide. *Science* **263**, 1615-1618 (1994).

22.   Q. Hu, C. R. Bazemore Walker, C. Girao, J. T. Opferman, J. Sun, J. Shabanowitz, D. F. Hunt, P. G. Ashton-Rickardt, Specific recognition of thymic self-peptides induces the positive selection of cytotoxic T lymphocytes. *Immunity* **7**, 221-231 (1997).

23.   B. T. Ober, Q. Hu, J. T. Opferman, S. Hagevik, N. Chiu, C. R. Wang, P. G. Ashton-Rickardt, Affinity of thymic self-peptides for the TCR determines the selection of CD8(+) T lymphocytes in the thymus. *Int Immunol* **12**, 1353-1363 (2000).

24. A. J. Leishman, L. Gapin, M. Capone, E. Palmer, H. R. MacDonald, M. Kronenberg, H. Cheroutre, Precursors of functional MHC class I- or class II-restricted CD8alphaalpha(+) T cells are positively selected in the thymus by agonist self-peptides. *Immunity* **16**, 355-364 (2002).

25. T. Yamagata, D. Mathis, C. Benoist, Self-reactivity in thymic double-positive cells commits cells to a CD8 alpha alpha lineage with characteristics of innate immune cells. *Nat Immunol* **5**, 597-605 (2004).

26. L. Wyss, B. D. Stadinski, C. G. King, S. Schallenberg, N. I. McCarthy, J. Y. Lee, K. Kretschmer, L. M. Terracciano, G. Anderson, C. D. Surh, E. S. Huseby, E. Palmer, Affinity for self antigen selects Treg cells with distinct functional properties. *Nat Immunol* **17**, 1093-1101 (2016).

27. K. A. Hogquist, S. C. Jameson, M. J. Bevan, Strong agonist ligands for the T cell receptor do not mediate positive selection of functional CD8+ T cells. *Immunity* **3**, 79-86 (1995).

28. E. Sebzda, S. Mariathasan, T. Ohteki, R. Jones, M. F. Bachmann, P. S. Ohashi, Selection of the T cell repertoire. *Annu Rev Immunol* **17**, 829-874 (1999).

29. S. Mariathasan, R. G. Jones, P. S. Ohashi, Signals involved in thymocyte positive and negative selection. *Semin Immunol* **11**, 263-272 (1999).

30. J. D. Mintern, M. M. Maurice, H. L. Ploegh, E. Schott, Thymic selection and peripheral activation of CD8 T cells by the same class I MHC/peptide complex. *J Immunol* **172**, 699-708 (2004).

31. V. P. Dave, Z. Cao, C. Browne, B. Alarcon, G. Fernandez-Miguel, J. Lafaille, A. de la Hera, S. Tonegawa, D. J. Kappes, CD3 delta deficiency arrests development of the alpha beta but not the gamma delta T cell lineage. *Embo J* **16**, 1360-1370 (1997).

32. P. Delgado, E. Fernandez, V. Dave, D. Kappes, B. Alarcon, CD3delta couples T-cell receptor signalling to ERK activation and thymocyte positive selection. *Nature* **406**, 426-430 (2000).

33. B. T. Backstrom, U. Muller, B. Hausmann, E. Palmer, Positive selection through a motif in the alphabeta T cell receptor. *Science* **281**, 835-838 (1998).

34. G. Werlen, B. Hausmann, E. Palmer, A motif in the alphabeta T-cell receptor controls positive selection by modulating ERK activity. *Nature* **406**, 422-426 (2000).

35. M. A. Daniels, E. Teixeiro, J. Gill, B. Hausmann, D. Roubaty, K. Holmberg, G. Werlen, G. A. Hollander, N. R. Gascoigne, E. Palmer, Thymic selection threshold defined by compartmentalization of Ras/MAPK signalling. *Nature* **444**, 724-729 (2006).

36. K. A. Swan, J. Alberola-Ila, J. A. Gross, M. W. Appleby, K. A. Forbush, J. F. Thomas, R. M. Perlmutter, Involvement of p21ras distinguishes positive and negative selection in thymocytes. *EMBO J* **14**, 276-285 (1995).

37. J. Alberola-Ila, K. A. Hogquist, K. A. Swan, M. J. Bevan, R. M. Perlmutter, Positive and negative selection invoke distinct signaling pathways. *J Exp Med* **184**, 9-18 (1996).

38. C. C. O'Shea, T. Crompton, I. R. Rosewell, A. C. Hayday, M. J. Owen, Raf regulates positive selection. *Eur J Immunol* **26**, 2350-2355 (1996).

39. T. W. McKeithan, Kinetic proofreading in T-cell receptor signal transduction. *Proc Natl Acad Sci U S A* **92**, 5042-5046 (1995).

40. S. E. Smith, S. C. Neier, B. K. Reed, T. R. Davis, J. P. Sinnwell, J. E. Eckel-Passow, G. F. Sciallis, C. N. Wieland, R. R. Torgerson, D. Gil, C. Neuhauser, A. G. Schrum, Multiplex matrix network analysis of protein complexes in the human TCR signalosome. *Science signaling* **9**, rs7 (2016).

41. L. K. Ely, K. J. Green, T. Beddoe, C. S. Clements, J. J. Miles, S. P. Bottomley, D. Zernich, L. Kjer-Nielsen, A. W. Purcell, J. McCluskey, J. Rossjohn, S. R. Burrows, Antagonism of antiviral and allogeneic activity of a human public CTL clonotype by a single altered peptide ligand: implications for allograft rejection. *J Immunol* **174**, 5593-5601 (2005).

42. T. Beddoe, Z. Chen, C. S. Clements, L. K. Ely, S. R. Bushell, J. P. Vivian, L. Kjer-Nielsen, S. S. Pang, M. A. Dunstone, Y. C. Liu, W. A. Macdonald, M. A. Perugini, M. C.

Wilce, S. R. Burrows, A. W. Purcell, T. Tiganis, S. P. Bottomley, J. McCluskey, J. Rossjohn, Antigen ligation triggers a conformational change within the constant domain of the alphabeta T cell receptor. *Immunity* **30**, 777-788 (2009).

43. W. A. Macdonald, Z. Chen, S. Gras, J. K. Archbold, F. E. Tynan, C. S. Clements, M. Bharadwaj, L. Kjer-Nielsen, P. M. Saunders, M. C. Wilce, F. Crawford, B. Stadinsky, D. Jackson, A. G. Brooks, A. W. Purcell, J. W. Kappler, S. R. Burrows, J. Rossjohn, J. McCluskey, T cell allorecognition via molecular mimicry. *Immunity* **31**, 897-908 (2009).

44. R. T. Abraham, A. Weiss, Jurkat T cells and development of the T-cell receptor signalling paradigm. *Nat Rev Immunol* **4**, 301-308 (2004).

45. K. A. Hogquist, S. C. Jameson, W. R. Heath, J. L. Howard, M. J. Bevan, F. R. Carbone, T cell receptor antagonist peptides induce positive selection. *Cell* **76**, 17-27 (1994).

46. H. E. Stefanski, D. Mayerova, S. C. Jameson, K. A. Hogquist, A low affinity TCR ligand restores positive selection of CD8+ T cells in vivo. *J Immunol* **166**, 6602-6607 (2001).

47. A. Weiss, J. D. Stobo, Requirement for the coexpression of T3 and the T cell antigen receptor on a malignant human T cell line. *J Exp Med* **160**, 1284-1299 (1984).

48. H. S. Azzam, A. Grinberg, K. Lui, H. Shen, E. W. Shores, P. E. Love, CD5 expression is developmentally regulated by T cell receptor (TCR) signals and TCR avidity. *J Exp Med* **188**, 2301-2311 (1998).

49. P. Wettstein, M. Strausbauch, T. Therneau, N. Borson, The application of real-time PCR to the analysis of T cell repertoires. *Nucleic Acids Res* **36**, e140 (2008).

50. S. L. Johnston, P. J. Wettstein, T cell receptor diversity in CTLs specific for the CTT-1 and CTT-2 minor histocompatibility antigens. *J Immunol* **159**, 2606-2615 (1997).

51. P. J. Wettstein, M. Strausbauch, N. Borson, Repertoires of T cell receptors expressed by graft-infiltrating T cells evolve during long-term recall responses to single minor histocompatibility antigens. *Int Immunol* **19**, 523-534 (2007).

52. E. M. Carmona, A. H. Limper, Update on the diagnosis and treatment of Pneumocystis pneumonia. *Therapeutic advances in respiratory disease* **5**, 41-59 (2011).

53. P. D. Murray, K. D. Pavelko, J. Leibowitz, X. Lin, M. Rodriguez, CD4(+) and CD8(+) T cells make discrete contributions to demyelination and neurologic disease in a viral model of multiple sclerosis. *J Virol* **72**, 7320-7329 (1998).

54. A. Ferrer, A. G. Schrum, D. Gil, A PCR-Based Method to Genotype Mice Knocked Out for All Four CD3 Subunits, the Standard Recipient Strain for Retrogenic TCR/CD3 Bone Marrow Reconstitution Technology. *BioResearch open access* **2**, 222-226 (2013).

55. J. Sloan-Lancaster, P. M. Allen, Altered peptide ligand-induced partial T cell activation: molecular mechanisms and role in T cell biology. *Annu Rev Immunol* **14**, 1-27 (1996).

56. D. M. La Face, C. Couture, K. Anderson, G. Shih, J. Alexander, A. Sette, T. Mustelin, A. Altman, H. M. Grey, Differential T cell signaling induced by antagonist peptide-MHC complexes and the associated phenotypic responses. *J Immunol* **158**, 2057-2064. (1997).

57. E. N. Kersh, A. S. Shaw, P. M. Allen, Fidelity of T cell activation through multistep T cell receptor zeta phosphorylation. *Science* **281**, 572-575 (1998).

58. G. J. Kersh, E. N. Kersh, D. H. Fremont, P. M. Allen, High- and low-potency ligands with similar affinities for the TCR: the importance of kinetics in TCR signaling. *Immunity* **9**, 817-826 (1998).

59. J. D. Rabinowitz, C. Beeson, C. Wulfing, K. Tate, P. M. Allen, M. M. Davis, H. M. McConnell, Altered T cell receptor ligands trigger a subset of early T cell signals. *Immunity* **5**, 125-135. (1996).

60. G. P. Morris, P. M. Allen, How the TCR balances sensitivity and specificity for the recognition of self and pathogens. *Nat Immunol* **13**, 121-128 (2012).

61. J. Zikherman, C. Jenne, S. Watson, K. Doan, W. Raschke, C. C. Goodnow, A. Weiss, CD45-Csk phosphatase-kinase titration uncouples basal and inducible T cell receptor signaling during thymic development. *Immunity* **32**, 342-354 (2010).

62. J. R. Schoenborn, Y. X. Tan, C. Zhang, K. M. Shokat, A. Weiss, Feedback circuits monitor and adjust basal Lck-dependent events in T cell receptor signaling. *Science signaling* **4**, ra59 (2011).

63. F. Wang, K. Beck-Garcia, C. Zorzin, W. W. Schamel, M. M. Davis, Inhibition of T cell receptor signaling by cholesterol sulfate, a naturally occurring derivative of membrane cholesterol. *Nat Immunol* **17**, 844-850 (2016).

64. O. Stepanek, A. S. Prabhakar, C. Osswald, C. G. King, A. Bulek, D. Naeher, M. Beaufils-Hugot, M. L. Abanto, V. Galati, B. Hausmann, R. Lang, D. K. Cole, E. S. Huseby, A. K. Sewell, A. K. Chakraborty, E. Palmer, Coreceptor scanning by the T cell receptor provides a mechanism for T cell tolerance. *Cell* **159**, 333-345 (2014).

65. E. Palmer, D. Naeher, Affinity threshold for thymic selection through a T-cell receptor-co-receptor zipper. *Nat Rev Immunol* **9**, 207-213 (2009).

66. J. E. Toettcher, O. D. Weiner, W. A. Lim, Using optogenetics to interrogate the dynamic control of signal transmission by the Ras/Erk module. *Cell* **155**, 1422-1434 (2013).

67. L. Kjer-Nielsen, C. S. Clements, A. W. Purcell, A. G. Brooks, J. C. Whisstock, S. R. Burrows, J. McCluskey, J. Rossjohn, A structural basis for the selection of dominant alphabeta T cell receptors in antiviral immunity. *Immunity* **18**, 53-64 (2003).

68. J. Rossjohn, S. Gras, J. J. Miles, S. J. Turner, D. I. Godfrey, J. McCluskey, T cell antigen receptor recognition of antigen-presenting molecules. *Annu Rev Immunol* **33**, 169-200 (2015).

69. J. Holst, K. M. Vignali, A. R. Burton, D. A. Vignali, Rapid analysis of T-cell selection in vivo using T cell-receptor retrogenic mice. *Nat Methods* **3**, 191-197 (2006).

70. L. Madsen, N. Labrecque, J. Engberg, A. Dierich, A. Svejgaard, C. Benoist, D. Mathis, L. Fugger, Mice lacking all conventional MHC class II genes. *Proc Natl Acad Sci U S A* **96**, 10338-10343 (1999).

71. A. G. Schrum, L. A. Turka, The proliferative capacity of individual naive CD4(+) T cells is amplified by prolonged T cell antigen receptor triggering. *J Exp Med* **196**, 793-803 (2002).

72. R. J. Stiles, A. G. Schrum, D. Gil, A co-housing strategy to improve fecundity of mice in timed matings. *Lab animal* **42**, 62-65 (2013).

73. M. L. Lobo, F. Esteves, B. de Sousa, F. Cardoso, M. T. Cushion, F. Antunes, O. Matos, Therapeutic potential of caspofungin combined with trimethoprim-sulfamethoxazole for pneumocystis pneumonia: a pilot study in mice. *PLoS One* **8**, e70619 (2013).

74. F. E. Lund, M. Hollifield, K. Schuer, J. L. Lines, T. D. Randall, B. A. Garvy, B cells are required for generation of protective effector and memory CD4 cells in response to Pneumocystis lung infection. *J Immunol* **176**, 6147-6154 (2006).

75. C. Deb, R. G. Lafrance-Corey, L. Zoecklein, L. Papke, M. Rodriguez, C. L. Howe, Demyelinated axons and motor function are protected by genetic deletion of perforin in a mouse model of multiple sclerosis. *Journal of neuropathology and experimental neurology* **68**, 1037-1048 (2009).

Acknowledgments

Author contributions

SCN, AF, KMW, SEPS, AMHK, KDP, TRD, RJS, DMH, and AGS performed experiments. SCN, AF, KMW, SEPS, AMH, KDP, JMC, EMC, AHL, AJJ, PJW, LRP, MAD, CN, DG, and AGS performed experimental design, analysis, and/or interpretation. ZC, JM, SRB, and JR generated and contributed the LC13ab.huCD8ab.JRT3, C1R.B0801, and C1R.Kb cell lines used in this work. DJK contributed intellectual input and the CD3δ^0 mouse strain required for this work. SCN, AF, KMW, SEPS, and AGS wrote the manuscript. All authors reviewed and/or edited the manuscript. AGS conceived the project.
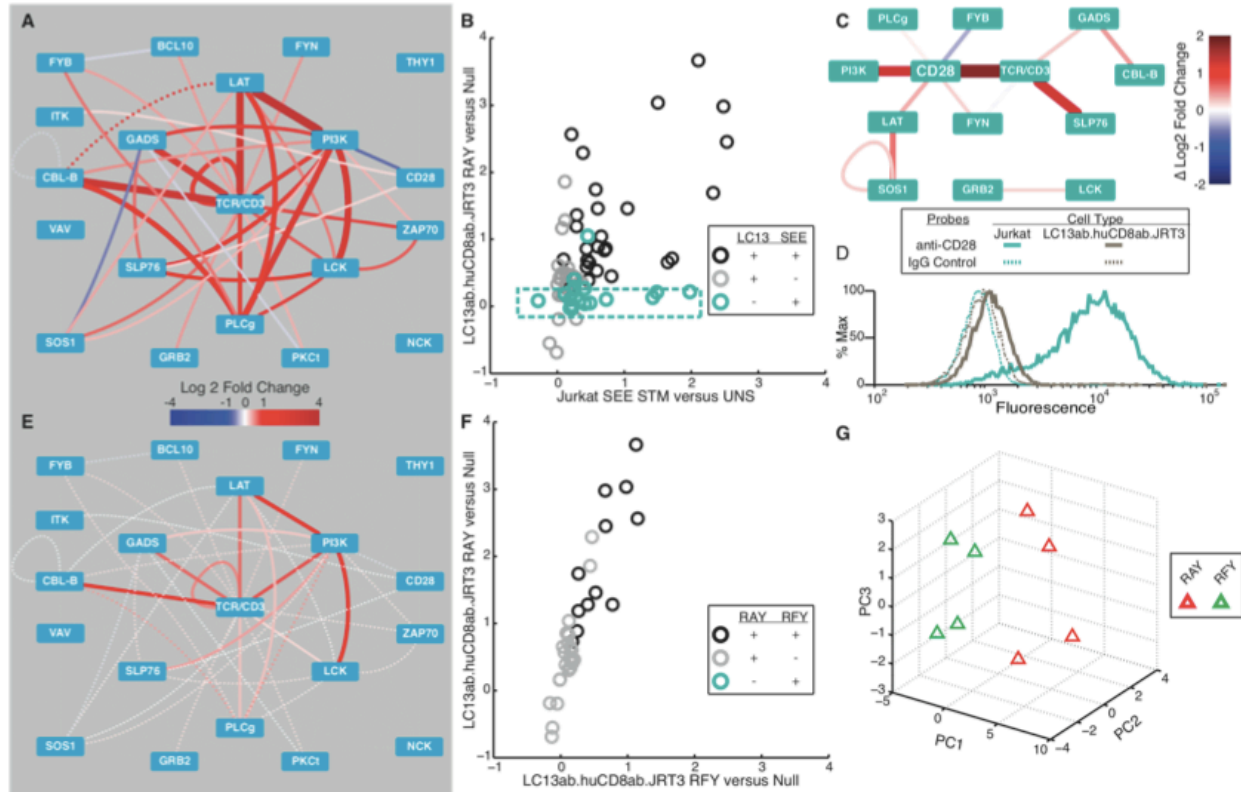
Figure Legends

Figure 1. PiSCES signatures reveal differential qualitative and quantitative TCR-proximal signaling activities. A) PiSCES signature of LC13ab.huCD8ab.JRT3 cells stimulated with agonist peptide (FLRG<u>RAY</u>GL) for 5-minutes (mean-log2 fold-change, stimulated/basal; dotted lines indicate trend of non-significant protein pairs that appear as hits for data comparisons shown ahead). **B)** Comparison of mean-log2 fold-changes in abundance of protein pair hits induced by agonist pMHC in LC13ab.huCD8ab.JRT3 cells versus SEE superantigen in Jurkat cells. Statistically significant hits that occurred in both stimuli are black, hits in LC13 system only are gray, and hits in SEE-Jurkat system are teal. **C)** Sub-network (from panel B, teal points within the teal dashed box) visualized as the difference in mean-log2 fold-change in SEE versus LC13. **D)** Surface staining with anti-CD28 or IgG negative control for Jurkat versus LC13ab.huCD8ab.JRT3 cells. **E)** PiSCES signature of LC13ab.huCD8ab.JRT3 cells stimulated with antagonist peptide (FLRG<u>RFY</u>GL) for 5-minutes (mean-log2 fold-change, stimulated/basal;

dotted lines indicate trend of non-significant protein pairs). **F)** Comparison of mean-log2 fold-changes in abundance of protein pair hits induced by LC13 agonist versus antagonist stimulation. Compared to B, note lack of teal "antagonist-only" hits. **G)** PCA of four independent experiments shows separation of 5-minute-agonist versus antagonist PiSCES signatures.
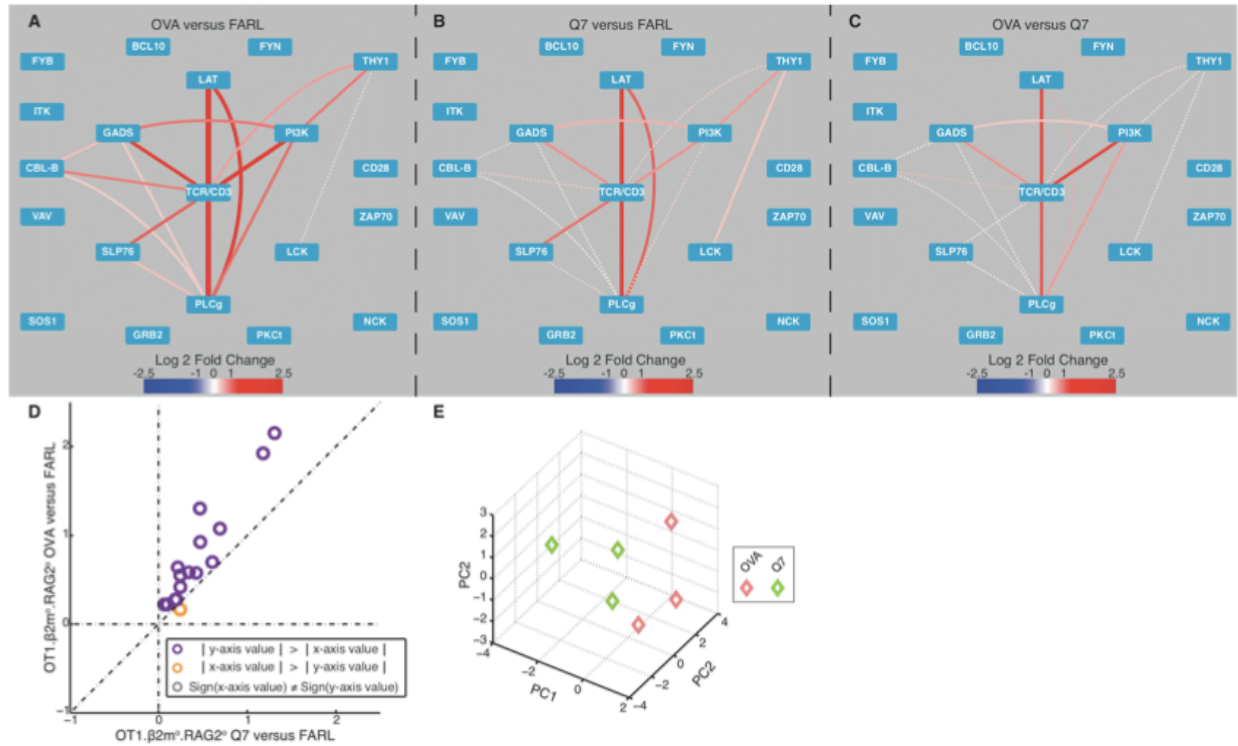
Figure 2. Predominant quantitative difference in PiSCES signatures comparing OT1 thymocyte response to positive and negative selection pMHC ligands. PiSCES signature of pre-selection OT1.β2mᵒ.RAG2ᵒ thymocytes stimulated for 1 minute with **A)** a negative selection peptide, OVA (mean-log2 fold-change, OVA/FARL conditions), or **B)** a positive selection peptide, Q7 (mean-log2 fold-change, Q7/FARL conditions). **C)** PiSCES signature when response to OVA is directly normalized to the response to Q7 (mean-log2 fold-change, OVA/Q7 conditions). Dotted lines in (A-C) indicate trend of non-significant protein pairs that appear as hits in any of the three experimental comparisons performed. **D)** Comparison of mean-log2 fold-changes in abundance of protein pair hits induced by OVA versus Q7 in pre-selection OT1.β2mᵒ.RAG2ᵒ thymocytes. Data points are displayed for hits that were statistically significant in any of the OVA versus FARL, Q7 versus FARL, or OVA versus Q7 comparisons. A separate trajectory of orange points (Y-axis value > X-axis value) that would clearly indicate

positive selection-specific protein complexes is not observed. **E)** PCA of three independent experiments shows separation of 1-minute OVA/FARL versus Q7/FARL PiSCES signatures.
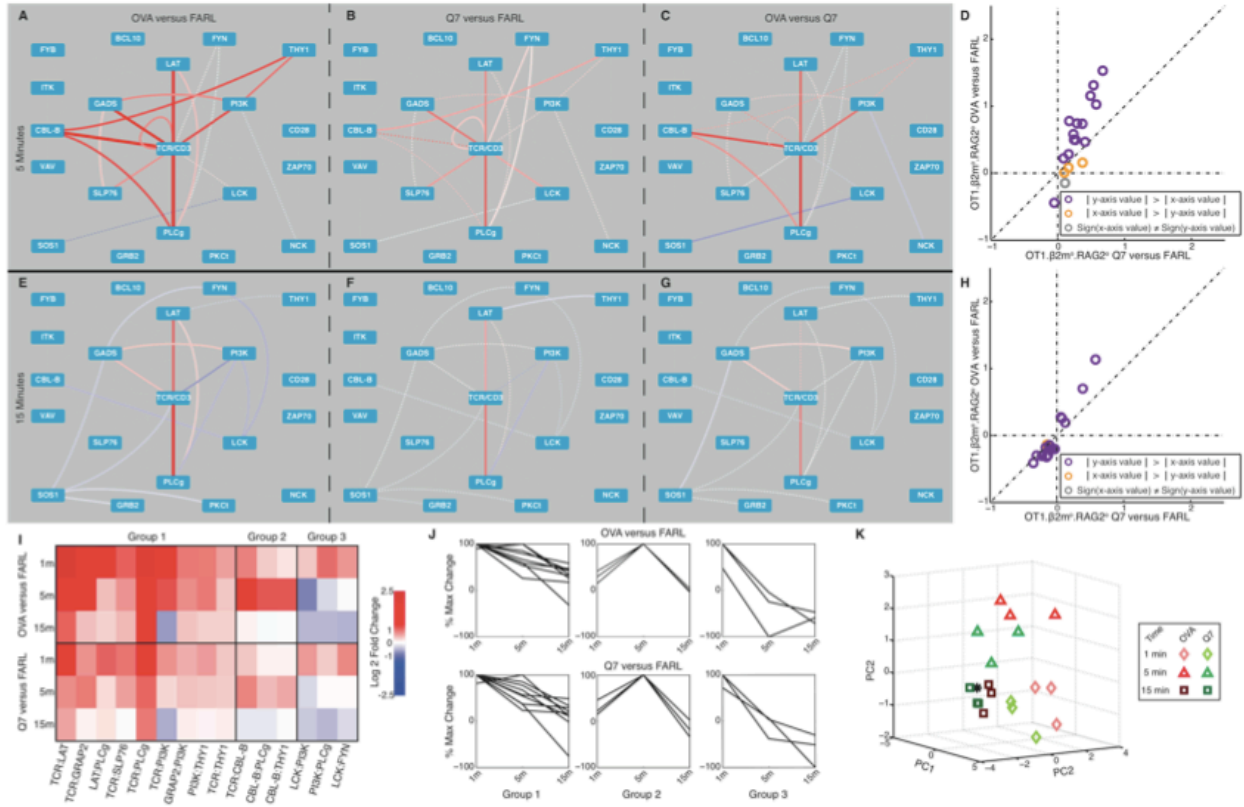
Figure 3. Kinetics of PiSCES signatures for positive and negative selection stimuli. PiSCES signatures of pre-selection OT1.β2m⁰.RAG2⁰ thymocytes stimulated for 5 minutes (A-D) or 15 minutes (E-H) with **A,E)** negative selection peptide, OVA (mean-log2 fold-change, OVA/FARL conditions; dotted lines indicate trend of non-significant protein pairs across a given time point), or **B,F)** positive selection peptide, Q7 (mean-log2 fold-change, Q7/FARL conditions). **C,G)** PiSCES signatures when response to OVA is directly normalized to the response to Q7 (mean-log2 fold-change, OVA/Q7 conditions). **D,H)** Comparisons of mean-log2 fold-changes in abundance of protein pair hits induced by OVA versus Q7 in pre-selection OT1.β2m⁰.RAG2⁰ thymocytes. Data points are displayed for hits that were statistically significant in any of the OVA versus FARL, Q7 versus FARL, or OVA versus Q7 comparisons. A separate trajectory of orange points (Y-axis value > X-axis value) that would clearly indicate positive selection-specific protein complexes is not observed. **I,J)** K-means clustering was performed using

percent-maximum log2 fold changes to define three kinetic patterns observed among the top 15 hits in response to OVA stimulation, categorized in groups 1-3. **I)** A kinetic heat map of the log2 fold changes is shown for these hits defined by the OVA stimulation condition. The matching data points in response to Q7 stimulation were observed to display similar kinetic behavior, but lower intensity fold-changes than those induced by OVA stimulation. **J)** K-means clustering data displayed as percent-maximum log2 fold change shows that the three kinetic behavior groups defined by response to OVA stimulation (top) also described the overall kinetic behavior of the same protein pairs in response to Q7 stimulation (bottom). **K)** With experimental n = 3 per time point, data across 1, 5, and 15 minute time points were used to generate a kinetic PCA matrix. Subjectively, it appears that data for response to OVA versus Q7 are distinguishable but relatively close to each other at each time point, with the time point of stimulation playing a major role in data placement in 3D analysis space, and OVA data appearing farther than Q7 data from a zero-stimulation point (*).

A FARL 10µM
CD4 vs CD8β
4.66

B Q7 10µM
CD4 vs CD8β
64.5

C OVA 10µM
CD4 vs CD8β
2.28

D

FYB, BCL10, FYN, THY1, LAT, ITK, GADS, PI3K, CBL-B, TCR/CD3, CD28, VAV, ZAP70, SLP76, LCK, SOS1, PLCg, NCK, GRB2, PKC1

Log 2 Fold Change
2.5 to -2.5

E
PC1, PC2, PC3
OVA 0.75nm ▽   Q7 10µM ▽

F OVA 0.75nM - CD8αβ
CD4 vs CD8β
39.4

G OVA 0.75nM - CD8αα
CD8α vs CD8β
6.7 93.3

H OVA 3nM - CD8αβ
CD4 vs CD8β
12.3

I OVA 3nM - CD8αα
CD8α vs CD8β
39.8 60.2

J OT1.β2m°.RAG2°
Live CD8β SP cell count relative to FARL
p=0.0031
p=0.0091
FARL 0.75 nM, OVA 0.75 nM, Q7 10 nM, OVA 3 nM

Figure 4. PiSCES signature makes quantitative signaling prediction, which passes functional test in FTOC. (A-I) Fetal thymi of genotype OT1.RAG2^o.β2m^o were cultured for seven days in the presence of exogenous β2m and specific peptides at the stated concentrations. **A)** 10 μM FARL peptide loads with high affinity into H-2Kb, but has no functional affinity for the OT1 TCR and represents the background no-selection condition. **B)** 10 μM Q7 induces positive selection of a substantial portion of CD8 SP cells. **C)** 10 μM OVA induces deletion and loss of CD8+ cells. **(D,E)** Lowering the dose of OVA peptide to 0.75 nM makes its PiSCES signature almost indistinguishable from that of 10 μM Q7. **D)** When PiSCES data resulting from 5 minute stimulation of pre-selection OT1.β2m^o.RAG2^o thymocytes with 0.75 nM OVA was normalized to data from stimulation with 10 μM Q7, the signatures virtually cancel out, eliminating almost all hits (mean-log2 fold-change, OVA/Q7 comparison). **E)** PCA of PiSCES data in four experiments described in panel (D), where separation of the two stimulatory conditions is no longer observable. **F)** 0.75 nM OVA in FTOC induced positive selection of CD8 SP cells (P = 0.031, paired, two-tailed Student's t-test, where the two lobes of each of seven fetal thymi were separated for tissue culture, one lobe in 0.75 nM OVA and the paired lobe in 0.75 nM FARL (low-dose FARL not shown, but similar to (A)). **G)** Gating the data in (F) on CD4(-) cells, the positively selected CD8 SP cells were largely conventional αβ T cells marked by CD8αβ expression. **H)** Raising OVA concentration to 3 nM still induced positive selection of CD8 SP cells. **I)** Gating the data in (H) on CD4(-) cells, many of the positively selected cells were seen to represent unconventional CD8α+ CD8β- cells. **J)** Live CD8αβ SP T cell counts from two independent experiments (including the experiment depicted in panels A-I), with each FTOC normalized to the mean of its corresponding FARL 0.75 nM condition and reported as fold-change. Number of thymus lobes per condition: 9 (FARL 0.75 nM), 9 (OVA 0.75 nM), 4 (Q7 10 μM), 6 (OVA 3 nM). Unpaired, two-tailed Student's t-test, P < 0.05.
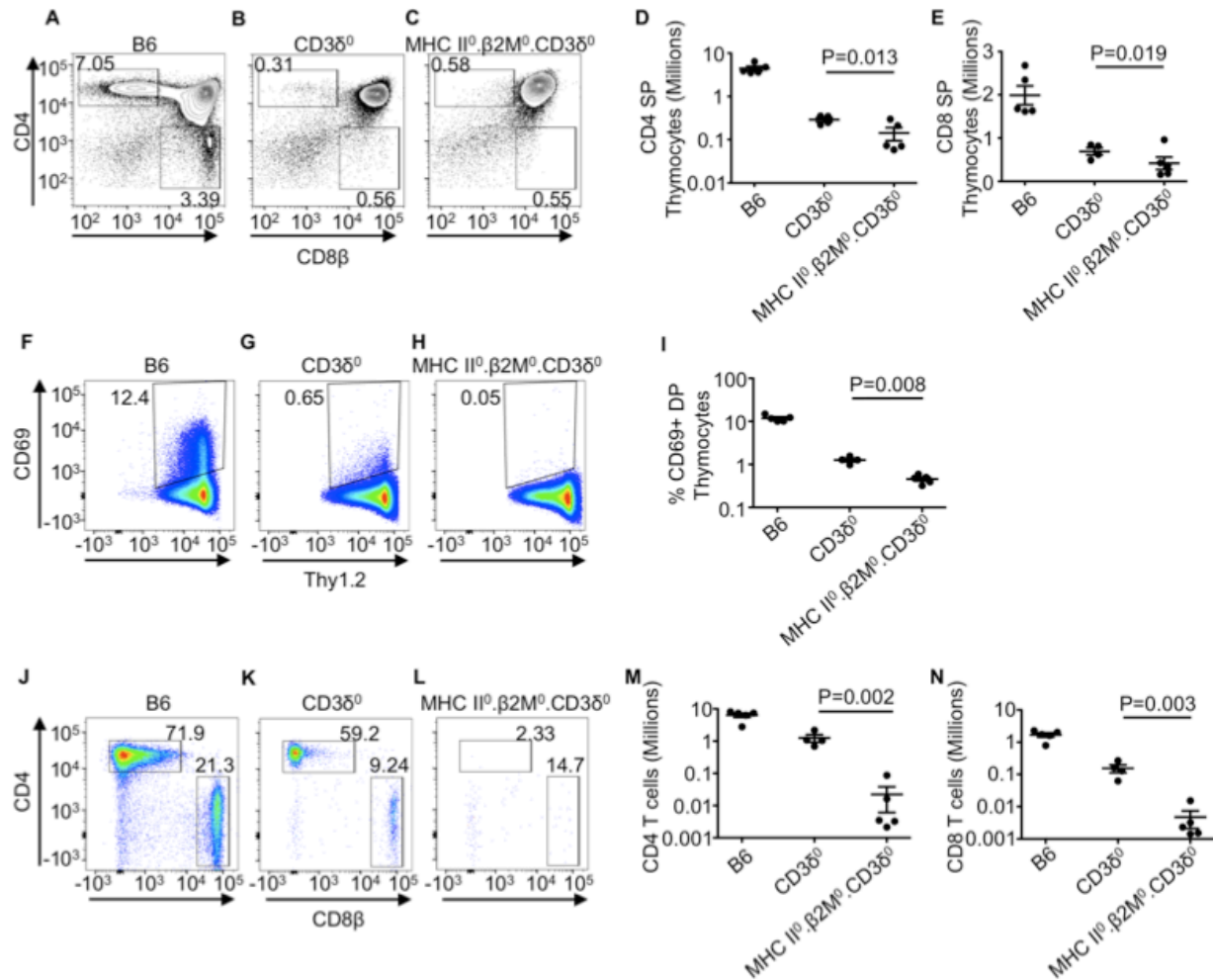
Figure 5. MHC-dependent signaling generates residual αβ T cells in CD3δ⁰ mice. Live Thy1.2+ thymocytes were analyzed for CD4 and CD8 surface expression by flow cytometry from the following genotypes, **(A)** wild-type B6, **(B)** CD3δ⁰ **(C)** MHC II⁰.β2m⁰.CD3δ⁰, and counts were obtained for **(D)** CD4 SP cells, and **(E)** CD8 SP cells. The percentage of CD4+ CD8+ DP thymocytes that were Thy1.2+ and CD69+ was obtained from the same three genotypes **(F-I)**. Live Thy1.2+ splenocytes were analyzed for CD4 and CD8 surface expression by flow cytometry from the same three genotypes **(J-L)**, and live counts were calculated for **(M)** CD4 T cells, and **(N)** CD8 T cells. Mouse n for splenocyte analysis was 4 or 5 per genotype. Statistical significance was determined by unpaired, two-tailed t-test, P < 0.05.
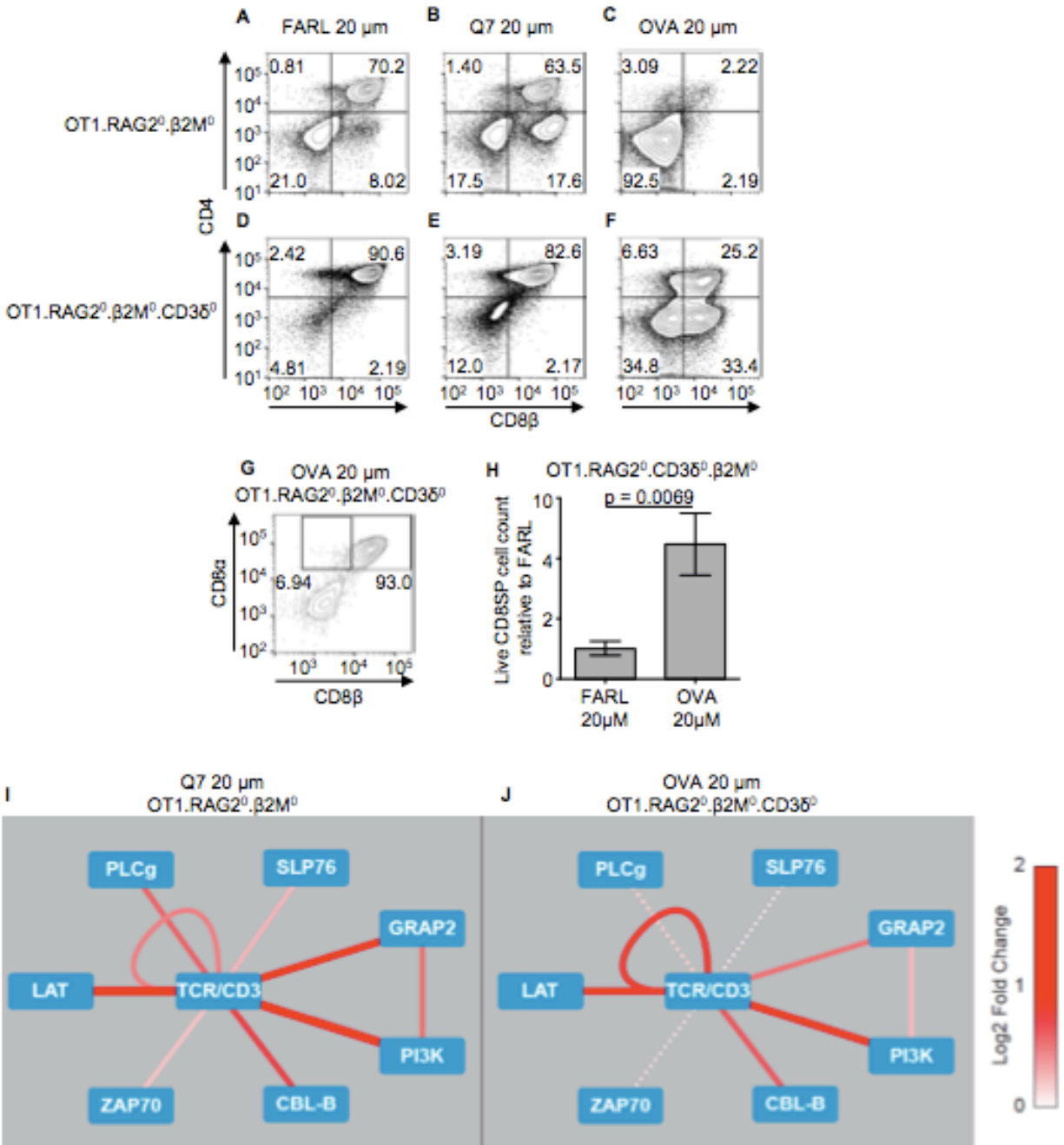
Figure 6. Positive selection signaling in the context of CD3δ°. **(A-G)** Fetal thymi were cultured for seven days in the presence of exogenous β2m (5 μg/mL) and specific peptides. For OT1.RAG2°.β2m° thymocytes (A-C), **(A)** 20 μM FARL peptide loads with high affinity into H-2Kb, but has no functional affinity for the OT1 TCR and represents the background no-selection condition. **(B)** 20 μM Q7 peptide can induce positive selection of a substantial portion of CD8

SP cells. **(C)** 20 μM OVA peptide induces deletion and loss of CD8+ cells. For

OT1.β2m°.RAG2°.CD3δ° thymocytes (D-G), **(D)** 20 μM FARL peptide is inert, and **(E)** Q7

peptide is inert, while **(F)** 20 μM OVA can induce positive selection of a substantial portion of

CD8 SP cells ($P < 0.0001$, unpaired, two-tailed Student's t-test comparing 12 thymic lobes

cultured in 20 μM OVA or 20 μM FARL). **(G)** The positively selected CD8 SP cells from the

OT1.β2m°.RAG2°.CD3δ° genotype were largely conventional αβ T cells as marked by CD8αβ

expression. **(H)** Live CD8αβ SP T cell counts from two independent experiments (including the

experiment depicted in panels A-G), with each FTOC normalized to the mean of its

corresponding FARL 20 μM condition and reported as fold-change. Number of thymus lobes per

condition: 7 (FARL 20 μM), 7 (OVA 20 μM). Unpaired, two-tailed Student's t-test, $P < 0.05$.

(I-J) PiSCES analysis of signaling proteins that join shared complexes in response to positive

selection pMHC antigens. **(I)** Induction of protein pairs from OT1.RAG2°.β2m° thymocytes when

assessing 5 minute stimulation with 20 μM Q7 peptide over negative-control FARL peptide. **(J)**

Induction of protein pairs from OT1.β2m°.RAG2°.CD3δ° thymocytes when assessing 5 minute

stimulation with 20 μM OVA peptide over negative-control FARL peptide.
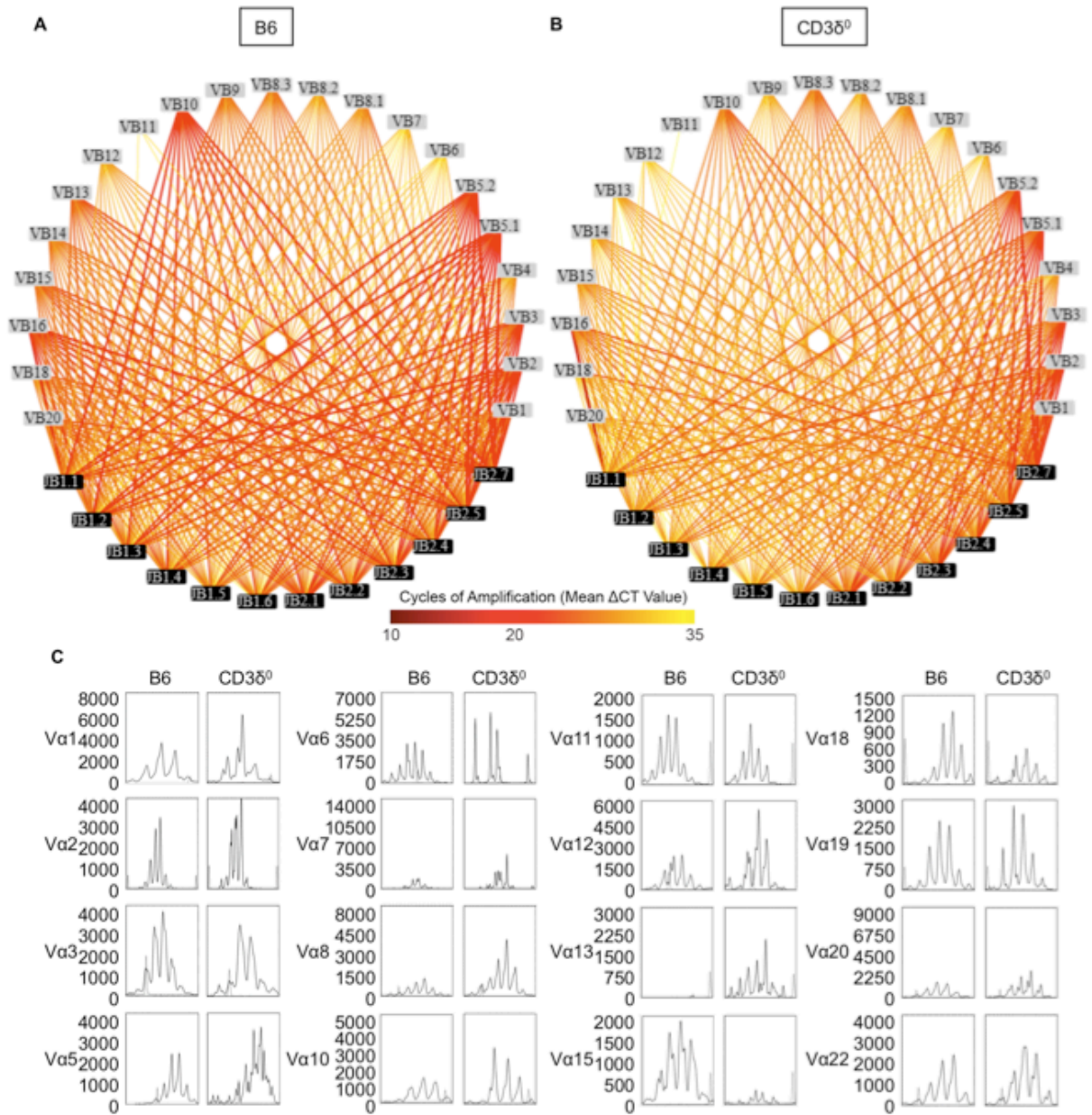
Figure 7. Diverse TCR repertoire in B6 and CD3δ° mice. A qPCR matrix-based method was utilized to assess relative representation of all possible TCRβ V-J combinations expressed as transcripts in splenocytes from **(A)** B6 or **(B)** CD3δ° mice. To approximate the maximum diversity generation potential per mouse for each genotype, the mean cycle threshold (Ct) value from the two mice with highest Shannon entropy for each genotype is displayed (top 2 of four B6 mice, top 2 of six CD3δ° mice tested, when 15 ng total splenic RNA was used as input). As

expected due to higher T cell representation among splenocytes, B6 transcripts for TCR were more abundant than was found in CD3δ°. Greater quantities of specific transcripts appear redder due to fewer PCR amplification cycles required to reach Ct, while lesser quantities of specific transcripts appear more yellow. All combinations that are displayed appeared at some positive level. **(C)** TCRα spectratyping was performed across a survey of V-genes expressed in splenocytes from B6 and CD3δ° mice. Each panel displays data from a single mouse (not pooled, from two mice per genotype tested).
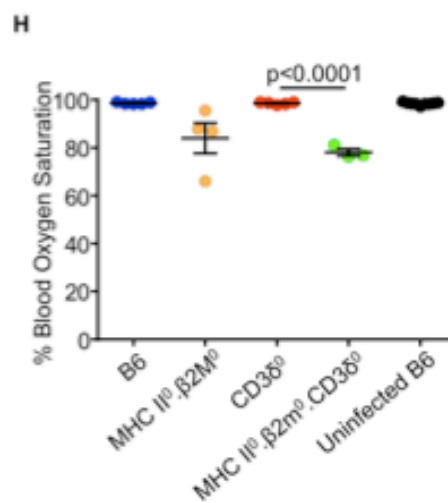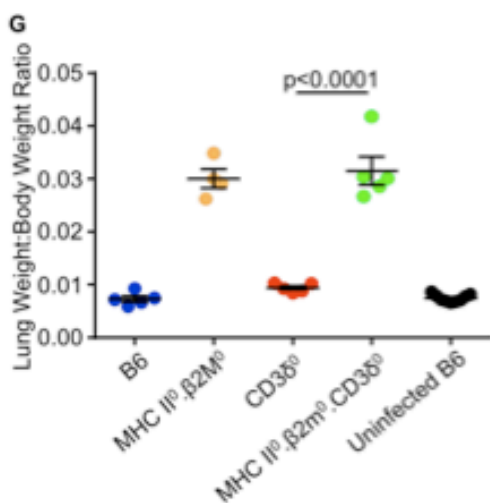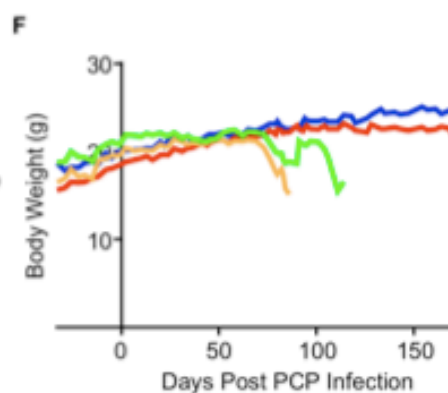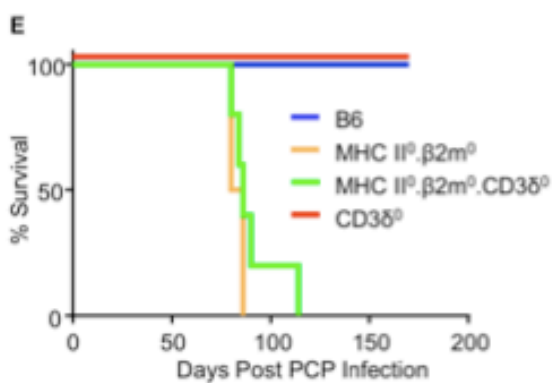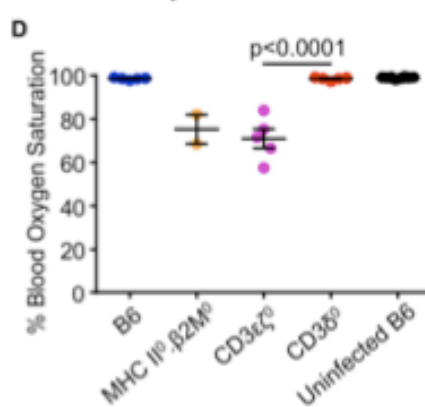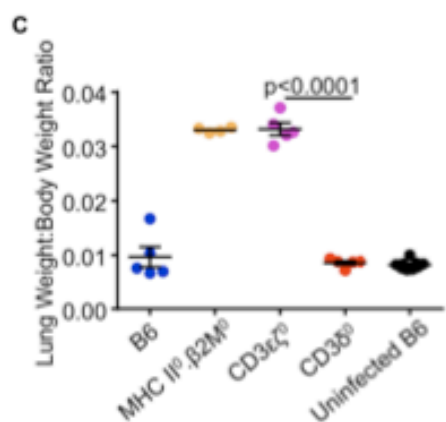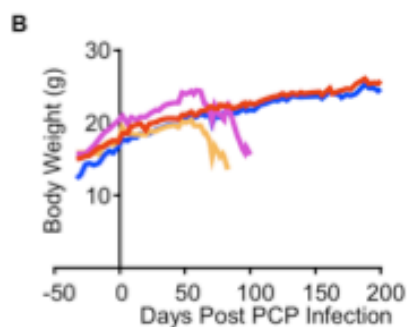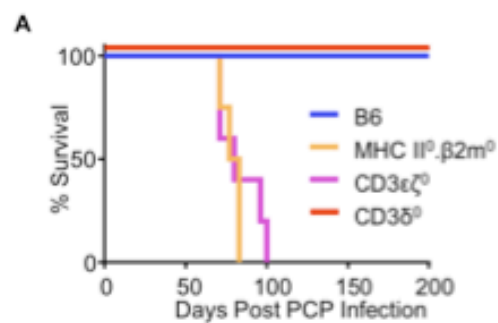
Figure 8. T cells in CD3δ° mice provide immune activity against PCP. (A-D) To assess the extent of T cell immune activity in a CD3δ° setting, mice from the listed genotypes were infected with *Pneumocystis* murina (mouse n ≥ 4 per genotype). **(A)** Kaplan-Meier curves display survival defined by mice being sacrificed upon loss of 20% weight, where CD3δ° was statistically different from susceptible genotypes (P = 0.004) by Log-Rank Mantel-Cox test. **(B)** Weight was monitored regularly throughout the experiment. **(C)** Upon sacrifice, lungs were harvested and weighed. **(D)** Just prior to sacrifice, blood oxygen saturation was measured for some of the mice. **(E-H)** To test the role of MHC in mediating protection from PCP in CD3δ° setting, mice from the listed genotypes were infected with PCP mouse n ≥ 4 per genotype). **(E)** Kaplan-Meier curves display survival defined by mice being sacrificed upon loss of 20% weight, where CD3δ° and MHC II°.β2m°.CD3δ° were statistically different (P = 0.014) by Log-Rank Mantel-Cox test. **(F)** Weight was monitored regularly throughout the experiment. **(G)** Upon sacrifice, lungs were harvested and weighed. **(H)** Just prior to sacrifice, blood oxygen saturation was measured for some of the mice. Unless otherwise specified, P-values denote statistical significance using unpaired, two-tailed Student's t-test, P < 0.05.
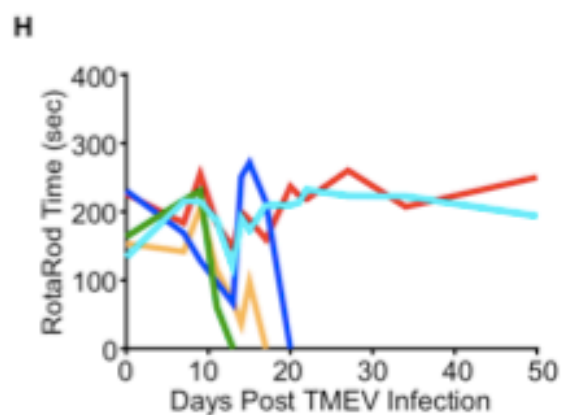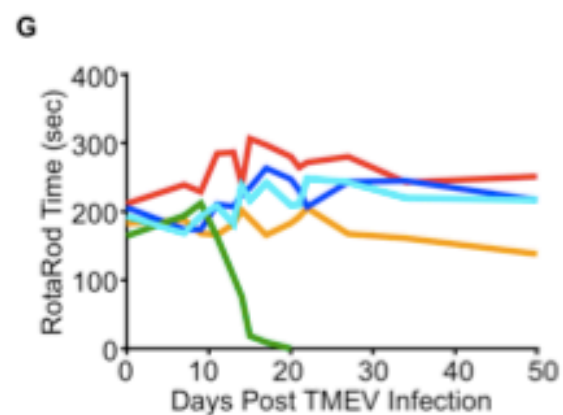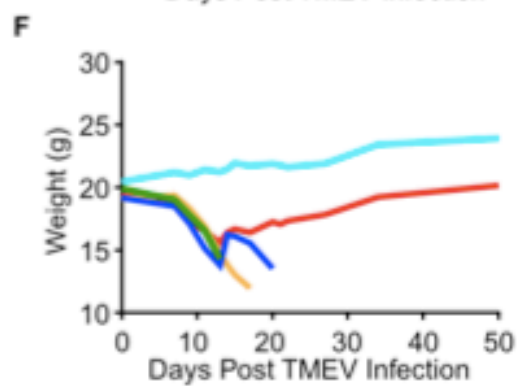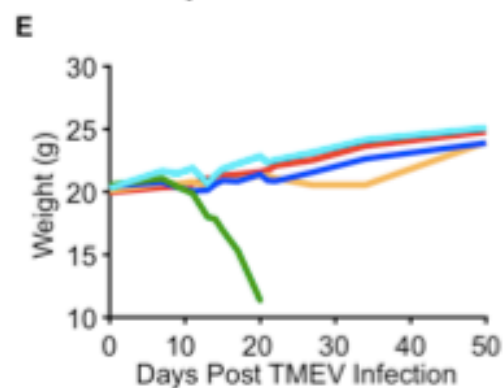
A. % Survival vs Days Post TMEV Infection. Legend: B6 (blue), CD3δ^0 (red), CD3$\epsilon\zeta^0$ (magenta), OT1.RAG2^0 (light green).

B. RotaRod Time (sec) vs Days Post TMEV Infection.

C. B6 — % Survival vs Days Post TMEV Infection. Legend: PBS (red), CD4 Depleted (GK1.5) (orange), CD8 Depleted (2.43) (blue), CD4 & CD8 Depleted (green), Uninfected (cyan).

D. CD3δ^0 — % Survival vs Days Post TMEV Infection.

E. Weight (g) vs Days Post TMEV Infection.

F. Weight (g) vs Days Post TMEV Infection.

G. RotaRod Time (sec) vs Days Post TMEV Infection.
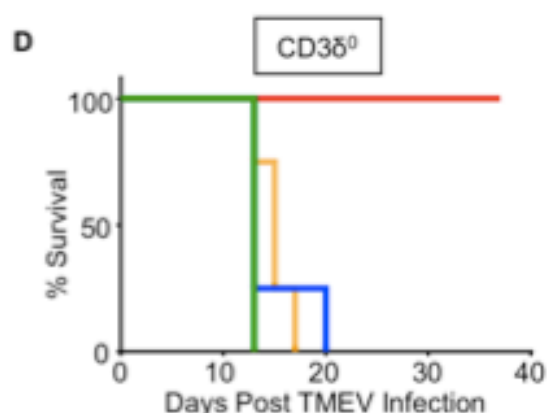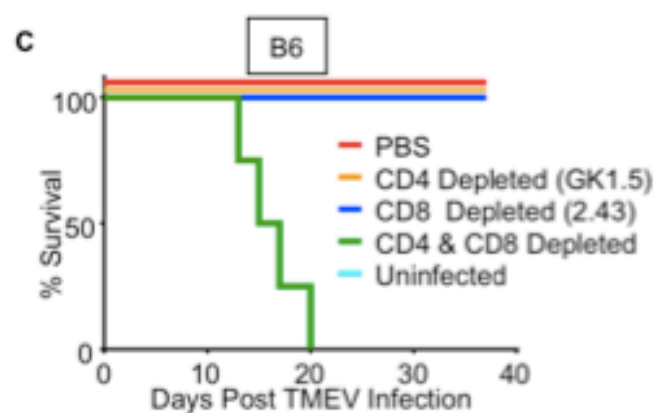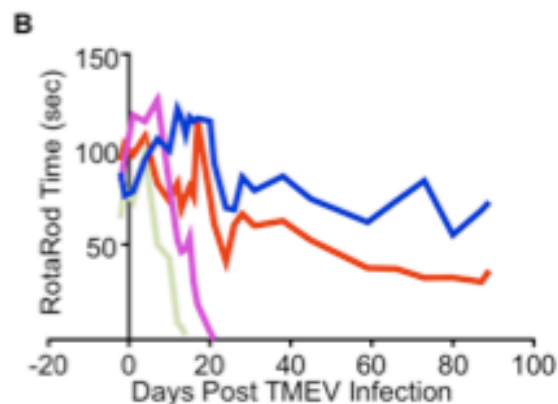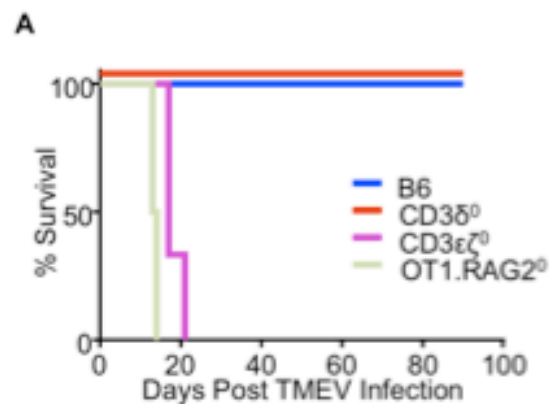
H. RotaRod Time (sec) vs Days Post TMEV Infection.

Figure 9. T cells in CD3δ° mice provide immune activity against TMEV. (A-B) To assess the extent of T cell immune activity in a CD3δ° setting, mice from the listed genotypes were infected with TMEV (mouse n ≥ 4 for all genotypes, except n=3 for CD3ε°ζ°). **(A)** Kaplan-Meier curves display survival defined by mice being sacrificed upon immobilization due to functional deficit or loss of 20% weight, where CD3δ° was statistically different from susceptible genotypes (P = 0.010) by Log-Rank Mantel-Cox test. **(B)** Functional deficit was monitored frequently throughout the experiment by RotaRod performance, measured as the average time elapsed prior to falling off the apparatus in two trials. **(C-H)** To assess CD4 and CD8 T cell immune activity, B6 and CD3δ° mice were either depleted of CD4 cells with GK1.5 anti-CD4 mAb injections, depleted of CD8 cells with 2.43 anti-CD8 mAb injections, depleted of both CD4 and CD8 cells, or were PBS-control injected as indicated, and were infected with TMEV (mouse n = 4 for all groups, except n=3 for CD3δ°+PBS). **(C-D)** Kaplan-Meier curves display survival defined by mice being sacrificed upon immobilization due to functional deficit or loss of 20% weight, where CD3δ° + PBS was statistically different from any of the three subset-depleted conditions (P = 0.008) by Log-Rank Mantel-Cox test. **(E-F)** Weight was monitored regularly throughout the experiment. **(G-H)** Functional deficit was monitored frequently throughout the experiment by RotaRod performance, measured as the average time elapsed prior to falling off the apparatus in two trials.